HHS Public Access

Author manuscript

Cell Rep. Author manuscript; available in PMC 2024 June 27.

Published in final edited form as:

Cell Rep. 2024 May 28; 43(5): 114229. doi:10.1016/j.celrep.2024.114229.

Modulation of GPR133 (ADGRD1) signaling by its intracellular interaction partner extended synaptotagmin 1

Gabriele Stephan[1,9], **Sara Haddock**[1,9], **Shuai Wang**[1,9], **Hediye Erdjument-Bromage**[2,8], **Wenke Liu**[3], **Niklas Ravn-Boess**[1], **Joshua D. Frenster**[1,4], **Devin Bready**[1], **Julia Cai**[1], **Rebecca Ronnen**[1], **Jonathan Sabio-Ortiz**[1], **David Fenyo**[3], **Thomas A. Neubert**[2,8], **Dimitris G. Placantonakis**[1,5,6,7,8,10,*]

[1]Department of Neurosurgery, NYU Grossman School of Medicine, New York, NY, USA

[2]Department of Neuroscience and Physiology, NYU Grossman School of Medicine, New York, NY 10016, USA

[3]Institute for Systems Genetics, NYU Grossman School of Medicine, New York, NY 10016, USA

[4]Department of Health and Experimental Sciences, Universitat Pompeu Fabra, 08003 Barcelona, Spain

[5]Laura and Isaac Perlmutter Cancer Center, NYU Grossman School of Medicine, New York, NY 10016, USA

[6]Kimmel Center for Stem Cell Biology, NYU Grossman School of Medicine, New York, NY 10016, USA

[7]Brain and Spine Tumor Center, NYU Grossman School of Medicine, New York, NY 10016, USA

[8]Neuroscience Institute, NYU Grossman School of Medicine, New York, NY 10016, USA

[9]These authors contributed equally

[10]Lead contact

SUMMARY

GPR133 (ADGRD1) is an adhesion G-protein-coupled receptor that signals through Gαs/cyclic AMP (cAMP) and is required for the growth of glioblastoma (GBM), an aggressive brain malignancy. The regulation of GPR133 signaling is incompletely understood. Here, we use

*Correspondence: dimitris.placantonakis@nyulangone.org.

AUTHOR CONTRIBUTIONS

Conceived and designed the experiments, G.S. and D.G.P.; performed the experiments, G.S., H.E.-B., W.L., S.W., N.R.-B., J.D.F., D.B., and J.C.; analyzed the data, G.S., H.E.-B., W.L., S.W., N.R.-B., and D.G.P.; wrote and edited the manuscript, G.S., H.E.-B., W.L., D.F., T.A.N., and D.G.P.

SUPPLEMENTAL INFORMATION

Supplemental information can be found online at https://doi.org/10.1016/j.celrep.2024.114229.

DECLARATION OF INTERESTS

D.G.P. and NYU Grossman School of Medicine own an EU and Hong Kong patent titled “Method for treating high-grade gliomas” on the use of GPR133 as a treatment target in glioma. D.G.P. and collaborators at NYU Grossman School of Medicine have filed a patent application titled “Anti-CD97 antibodies and antibody-drug conjugates”. D.G.P. has received consultant fees from Tocagen, Synaptive Medical, Monteris, Robeaute, Advantis, and Servier Pharmaceuticals.

proximity biotinylation proteomics to identify ESYT1, a Ca^{2+}-dependent mediator of endoplasmic reticulum-plasma membrane bridge formation, as an intracellular interactor of GPR133. ESYT1 knockdown or knockout increases GPR133 signaling, while its overexpression has the opposite effect, without altering GPR133 levels in the plasma membrane. The GPR133-ESYT1 interaction requires the Ca^{2+}-sensing C2C domain of ESYT1. Thapsigargin-mediated increases in cytosolic Ca^{2+} relieve signaling-suppressive effects of ESYT1 by promoting ESYT1-GPR133 dissociation. ESYT1 knockdown or knockout in GBM slows tumor growth, suggesting tumorigenic functions of ESYT1. Our findings demonstrate a mechanism for the modulation of GPR133 signaling by increased cytosolic Ca^{2+}, which reduces the signaling-suppressive interaction between GPR133 and ESYT1 to raise cAMP levels.

Graphical abstract

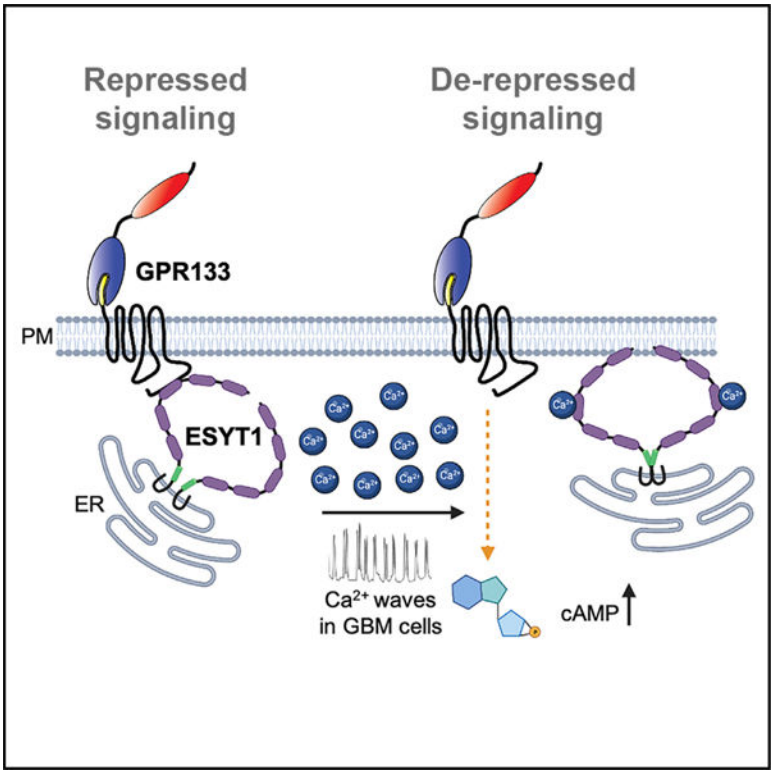

In brief

Stephan et al. use proximity biotinylation proteomics to identify an interaction between GPR133, an adhesion GPCR, and extended synaptotagmin 1 (ESYT1), a Ca^{2+}-dependent mediator of ER-plasma membrane bridges. ESYT1-driven repression of GPR133 signaling is relieved by increases in cytosolic Ca^{2+}. This interaction may be relevant to the pathogenesis of glioblastoma.

INTRODUCTION

The 32 members of the adhesion family of G-protein-coupled receptors (aGPCRs) have recently received attention for their roles in both physiological processes and disease.[1–6]

aGPCRs are characterized by an intracellular C terminus, seven transmembrane segments, and long extracellular N termini that adhere to components of the extracellular matrix or membrane proteins. These N termini contain receptor-specific domains that determine binding to extracellular interactors, as well as a conserved GPCR autoproteolysis inducing (GAIN) domain, which catalyzes autoproteolytic cleavage at the GPCR proteolysis site (GPS) to generate N-terminal (NTF) and C-terminal (CTF) fragments.[7,8] Immediately distal to the GPS lies the Stachel sequence, which has been shown by functional and structural data to act as an endogenous tethered agonist by binding an orthosteric binding groove within the seven-transmembrane portion of aGPCRs.[9–13] Several lines of evidence suggest that NTF-CTF dissociation may promote Stachel-dependent receptor activation, although it is not absolutely necessary.[8]

Signaling mechanisms entrained by aGPCRs are receptor specific and may also vary as a function of tissue and biological context. While some aGPCRs exhibit promiscuity in their coupling to G proteins, others demonstrate a dominant predilection for specific G proteins. Less is known about other intracellular regulatory mechanisms that influence trafficking to the cell membrane, signaling, and possible endocytosis, recycling, or desensitization.

We recently demonstrated that GPR133 (ADGRD1), a member of the aGPCR family, is crucial for tumor growth in glioblastoma (GBM), an aggressive primary brain malignancy.[8,14–18] GPR133 couples to Gαs to increase intracellular cyclic AMP (cAMP).[8,9,17–20] Our previous work has helped elucidate mechanisms of activation of GPR133.[8,17,18] GPR133 undergoes autoproteolytic cleavage at the GPS in the endoplasmic reticulum (ER).[8] The NTF and CTF remain non-covalently attached during receptor trafficking through the secretory pathway to the plasma membrane (PM), where NTF-CTF dissociation takes place.[8] Our working model posits that NTF-CTF dissociation at the PM promotes receptor signaling, even though an uncleavable GPR133 mutant (H543R) is still signaling competent, albeit at mildly reduced levels relative to wild-type (WT) GPR133.[8]

GPR133 manifests elevated basal levels of Gαs-mediated signaling[8,17–20]; however, the intracellular mechanisms that regulate GPR133 signaling and their impact on GBM pathogenesis are not understood. Here, we use proximity biotinylation proteomics to identify intracellular interactors in the vicinity of GPR133. We demonstrate that ESYT1 (extended synaptotagmin 1), an ER-associated protein that forms ER-PM tethers in a Ca^{2+}-dependent manner,[21–30] interacts with GPR133 to attenuate Gαs-mediated signaling in both HEK293 and patient-derived GBM stem cells (GSCs). This protein-protein interaction does not regulate trafficking of GPR133 to the PM. The ESYT1-mediated attenuation of GPR133 signaling depends on a Ca^{2+}-sensing C2 domain of ESYT1 and is relieved by increases in intracellular Ca^{2+}. ESYT1 knockdown (KD) or knockout (KO) in GSCs impairs tumor growth *in vitro* and to a lesser extent *in vivo*, suggesting that ESYT1 has other functions beyond regulation of GPR133 signaling. Overall, our findings suggest that ESYT1, an intracellular interactor of GPR133, regulates GPR133 signaling in a Ca^{2+}-dependent manner. This observation links Ca^{2+} flux to GPR133 signaling via Gαs and cAMP and establishes a paradigm for regulation of aGPCR activation by other cellular signaling mechanisms.

RESULTS

Identification of ESYT1 as intracellular interactor of GPR133

To identify intracellular interactors of GPR133, we used an approach combining proximity biotinylation, affinity purification, and mass spectrometry (MS; Figure 1A). We transfected HEK293T cells with GPR133 fused to a C-terminal BioID2,[31] which catalyzes biotinylation of intracellular proteins in close proximity to GPR133. In addition to the WT receptor (GPR133-BioID2), we included a cleavage-deficient and signaling-impaired double-mutant GPR133 (H543R/T545A-BioID2) in our study,[8,11,12,18] in order to identify both signaling-dependent and -independent interactors. Mutation of H543 to R prevents cleavage of GPR133 into NTF and CTF and mildly reduces receptor signaling.[8] An additional mutation at T545, representing the first residue of the endogenous Stachel sequence, is expected to abolish GPR133 signaling. Overexpression of both constructs in transfected HEK293T cells was confirmed by immunofluorescent staining and immunoblot (Figures S1A–S1C). Consistent with our previous findings,[8,18] both WT and mutant GPR133 were found not only at the PM, but also in intracellular compartments (ER, Golgi and the secretory pathway) (Figure S1A), a subcellular localization pattern that is required for trafficking of cell-surface proteins to the PM. The signaling capacity of BioID2-fused GPR133 was confirmed by quantifying cAMP levels using a homogeneous time-resolved fluorescence (HTRF)-based assay. Intracellular cAMP levels were significantly increased in cells overexpressing WT GPR133-BioID2, compared to the vector control or the signaling-deficient mutant H543R/T545A-BioID2 (Figure S1B). After treatment with biotin, immunoblotting for biotin indicated self-biotinylation of the BioID2 fusions (Figure S1C).

To identify intracellular GPR133 interactors, transfected HEK293T cells were treated with biotin, and biotinylated proteins were purified from whole-cell lysates using NeutrAvidin beads (Figure 1A). Samples were analyzed by western blot before (input) and after NeutrAvidin purification (elution) (Figure S1D). Proteins from the elution samples were further analyzed by MS (Figure 1A; Table S1). Our analysis identified 386 signaling-independent interactors that were robustly biotinylated by both WT and signaling-deficient mutant GPR133 compared to a control condition ($\log_{10}$ fold change >1 and $-\log_{10} p$ > 5) (Figures 1B and S2A; Table S2), as well as a few signaling-dependent proteins that preferentially associated with the signaling-competent WT GPR133 or the signaling-deficient H543R/T545A mutant (Figure S3; Table S3). Of note, we detected Gβ (Table S2) and Gα subunits (Table S1) as putative GPR133 interactors, a finding that inspired confidence in our approach. Gene set enrichment analysis (GSEA) of the 396 and 393 proteins enriched in the WT vs. control or mutant vs. control comparisons, respectively, identified enrichment of proteins related to hemostasis in the datasets of WT and mutant GPR133 interactors (Figure S2C).

We then decided to screen some of the most robustly biotinylated putative interactors. Our screening assays with ESYT1, one of the most robustly biotinylated proteins in HEK293T cells expressing either WT GPR133-BioID2 or H543R/T545A-BioID2 (Table S2; Table S1), validated it as a putative interactor. ESYT1 belongs to a family of evolutionarily conserved proteins (ESYT1–3 in mammals) that are associated with the ER and form ER-to-PM tethers

that mediate lipid exchange between the ER and the PM without fusion of the lipid bilayers. Such lipid transfer is mediated by homo- or heteromultimerization of members of the ESYT family through their synaptotagmin-like mitochondrial-lipid binding protein (SMP) domains[29] (Figure 1C, i). Among the mammalian ESYT proteins, ESYT1 is unique, because its ER-PM tethering function is Ca^{2+} dependent (Figure 1C, i and ii).[21–26,28,30] Overall, this finding raised the possibility that ESYT1 interacts with GPR133 regardless of the latter's signaling capacity.

To validate the structural interaction between GPR133 and ESYT1, we used a co-purification approach. We generated a stable cell line of HEK293T cells expressing WT GPR133 (WT) or a cleavage-deficient (H543R) GPR133 mutant, both tagged with a Twin-Strep-tag at the C terminus.[8,18] We transfected these cells with ESYT1 and prepared whole-cell lysates (Figure 1D, i). Western blot analysis confirmed expression of GPR133 and ESYT1. As expected, using an antibody against the GPR133 cytosolic C terminus, we detected a band corresponding to the cleaved GPR133 CTF (blue arrowhead, ~25 kDa) in cells overexpressing WT GPR133 and a band representing the uncleaved full-length receptor (red arrowhead, ~110 kDa) in cells overexpressing GPR133 H543R (Figure 1D, i).[8] A minor band representing a small fraction of uncleaved receptor was also seen in cells overexpressing WT GPR133, as expected (red arrowhead, Figure 1D, i).[8] Using an antibody against ESYT1, we identified bands corresponding to the predicted molecular weight of ESYT1 (black arrowheads, ~123 kDa). We were able to detect endogenous ESYT1 in empty-vector-transfected cells, as well as overexpression of exogenous ESYT1 in ESYT1-transfected cells (black arrowheads, Figure 1D, i). Next, we isolated Strep-tagged WT and H543R GPR133 by affinity purification using Strep-Tactin XT-coated magnetic beads. Western blot analysis of elution samples using an antibody against the GPR133 C terminus confirmed purification of the CTF (blue arrowhead, ~25 kDa) as well as small amounts of uncleaved full-length receptor (red arrowhead, ~110 kDa) from WT GPR133-overexpressing cells and only the full-length receptor (red arrowhead, ~110 kDa) in elution samples from cells overexpressing H543R GPR133 (Figure 1D, ii). Using an antibody against ESYT1, we detected bands corresponding to ESYT1 in elution samples of cells expressing WT or H543R GPR133 transfected with ESYT1 (black arrowheads, Figure 1D, ii). The co-purification of exogenous ESYT1 from cells expressing either WT or H543R GPR133 suggests that the ESYT1-GPR133 interaction does not depend on GPR133 cleavage.

We also screened two additional interactors that were significantly enriched in the comparisons to the control condition: OXSR1 (oxidative stress-responsive kinase 1), which was equivalently biotinylated in the WT and mutant GPR133 conditions (Table S2), and CYFIP2 (cytoplasmic FMR1-interacting protein 2), which was selectively biotinylated only in the WT GPR133 condition (Table S3; Figure S2B). Finally, as a control, we tested two additional proteins, NAE1 (NEDD8-activating enzyme E1 subunit 1) and RHOT2 (mitochondrial Rho GTPase 2), both of which were biotinylated only in the WT GPR133 condition, but did not meet our stringent criteria for enrichment relative to the control condition (Table S3; Figure S2B). In co-purification experiments using HEK293T cells co-transfected with WT GPR133 tagged at the C terminus with the Twin-Strep-tag and OXSR1, CYFIP2, NAE1, or RHOT2, tagged at the N terminus with the Myc epitope, we failed to

validate a structural interaction of the candidates with GPR133 (Figure S3). Co-expression of OXSR1, NAE1, and RHOT2 with GPR133 reduced GPR133 signaling (Figure S4A), but also reduced the cell-surface expression of GPR133 in ELISAs (Figure S4B), suggesting the effects were not related to modulation of receptor signaling, but rather protein stability or receptor trafficking. Furthermore, pharmacologic inhibition of NAE1 with MLN4924 (pevonedistat)[32] did not appreciably affect GPR133 signaling (Figure S4C). Collectively, these results encouraged further study of ESYT1, but not other screened candidates.

ESYT1 downregulates GPR133 signaling

We tested whether perturbation of ESYT1 levels in HEK293T cells affects GPR133 expression, trafficking to the PM, or signaling. To knock down ESYT1, we used HEK293T cells stably overexpressing GPR133 or an empty vector as control and transduced them with a lentiviral short hairpin RNA (shRNA) construct specific for targeting exon 8 of ESYT1 (shESYT1) or a non-specific scrambled control (shSCR) with no predicted targets in the genome. Western blot analysis confirmed reduced expression of ESYT1 following HEK293T cell transduction with shESYT1 compared to shSCR (Figures 2A, i, and S5). Overall GPR133 expression did not change in shESYT1-transduced cells compared to shSCR-transduced cells as shown by western blot of whole-cell lysates (Figures 2A, i and ii, and S5). Cell-surface expression of GPR133 at the PM was tested with ELISA of non-permeabilized cells, using an antibody against GPR133's N terminus.[8,17] GPR133 surface expression was not altered following ESYT1 KD compared to control (Figure 2B). In agreement with immunoblot and ELISA data, immunofluorescent staining of GPR133-overexpressing HEK293T cells showed the same overall subcellular localization pattern for GPR133 after transduction with shSCR or shESYT1 (Figure 2C). While ESYT1 KD had no effect on GPR133 expression levels or PM localization, cAMP levels of GPR133-expressing cells were significantly increased following ESYT1 KD, compared to control (Figure 2D).

In an alternative approach, we knocked out ESYT1 using CRISPR-Cas9 (Figures S6 and S7). HEK293T cell pools were lentivirally transduced with Cas9 and guide RNAs (gRNAs) specifically targeting either ESYT1 at exon 4 (Figure S6A) or the non-essential human *Rosa26* locus. To validate genome editing in the pool of HEK293T cells expressing the gRNA targeting *ESYT1*, we PCR-amplified the portion of the *ESYT1* gene targeted by the gRNA (exon 4) (Figures S6A and S6B) and subjected it to Sanger sequencing. Significant sequencing aberrations were found in the ESYT1-KO condition at the gRNA cut site, which were not found in control cells expressing the gRNA targeting *Rosa26* (Figure S6C). Tracking of indels by decomposition (TIDE)[33] demonstrated a 95.6% editing efficiency ($R^2 = 0.96$) in the ESYT1-KO pool; however, only 59.8% of indels were compatible with frameshift and KO. We therefore infer that only approximately 60% of *ESYT1* alleles in the ESYT1-KO pool encode a KO. However, the actual KO prevalence may be even higher if a 12 bp deletion we found (Figure S6D) extends to the intron/exon junction in the 5′ end of exon 4 to cause aberrant splicing.

A significant reduction of ESYT1 protein levels in the cell pool harboring the ESYT1-KO construct was observed by western blot, compared to the *Rosa26* control (Figures S7A, i, and S8). *Rosa26* control cells and ESYT1-KO cells were then transiently transfected with

a GPR133-expressing plasmid or an empty vector control, and GPR133 expression was assessed by western blot (Figures S7A, i, and S8). For unclear reasons, GPR133 expression levels in whole-cell lysates were mildly but consistently higher in ESYT1-KO cells relative to the *Rosa26* condition (Figure S7A, ii), despite transfection of equal amounts of plasmid across both conditions. However, GPR133 surface expression in ELISAs did not differ between the two conditions (Figure S7B). Using an antibody against the N terminus of GPR133 for immunofluorescent staining, we did not observe any differences in GPR133 subcellular localization between *Rosa26*- and ESYT1-KO cells (Figure S7C). Similar to ESYT1 KD, intracellular cAMP increased in GPR133-overexpressing cells following ESYT1 KO compared to the *Rosa26* condition (Figure S7D).

To rule out that enhanced GPR133 signaling in ESYT1-KO cells arose from the increase in its protein levels, we repeated similar experiments but transfected ESYT1-KO cells with a substantially lower amount of GPR133-expressing plasmid relative to *Rosa26* cells (1.5 μg vs. 3.5 μg, respectively) (Figures S7E–S7G and S8). These assays demonstrated that even when GPR133 protein was expressed equivalently in *Rosa26*- and ESYT1-KO cells, the KO of ESYT1 still resulted in a significant increase in GPR133 signaling.

In a complementary approach, we tested the effects of overexpression of ESYT1 on GPR133 signaling. We generated HEK293 cells stably overexpressing an ESYT1-GFP fusion protein and transfected them with GPR133. Western blots of whole-cell lysates confirmed overexpression of ESYT1 and GPR133 (Figure 2E, i). GPR133 expression or PM localization was not affected by ESYT1 overexpression, as seen by western blot, surface ELISA, and immunofluorescent staining (Figures 2E, ii–2G and S9). Immunofluorescence microscopy demonstrated co-localization of ESYT1-GFP and GPR133 immunoreactivity within intracellular compartments that likely represent the ER, Golgi apparatus, and secretory pathway (Figure 2G). In contrast to ESYT1 KD or KO, overexpression of ESYT1 led to a significant reduction in cAMP levels in GPR133-expressing cells (Figure 2H).

To determine whether the effects of the shRNA KD were specific to ESYT1, we tested whether overexpression of ESYT1 rescues the effect of ESYT1 KD on GPR133 signaling. We transduced HEK293T cells stably expressing GPR133 with shSCR or shESYT1 lentiviral constructs and then transfected them with exogenous ESYT1 or an empty vector control. Western blot analysis confirmed reduced ESYT1 levels in ESYT1 KD cells and increased ESYT1 expression in ESYT1-transfected cells (Figure 2I, i). GPR133 expression levels remained unchanged throughout these perturbations (Figure 2I, i and ii). In HTRF signaling assays, cAMP levels increased following KD of ESYT1, compared to the shSCR condition, while they decreased following overexpression of ESYT1 (Figure 2J). Importantly, ESYT1 overexpression rescued the increase in cAMP levels brought about by ESYT1 KD, suggesting specificity of the shRNA (Figure 2J).

Next, we set out to determine whether the modulation of intracellular cAMP levels by ESYT1 is specific to GPR133 and not due to effects on Gαs signaling or adenylate cyclase enzymatic activity. To test whether ESYT1 may interfere with Gαs signaling, we assessed ESYT1 effects on signaling by another Gαs-coupled receptor, the β2 adrenergic receptor (ADRB2). We transduced HEK293T cells with lentiviral shSCR or shESYT1 and

transfected them with a C-terminal FLAG-tagged ADRB2 or a vector control. Western blot analysis confirmed reduced ESYT1 expression in the KD condition and overexpression of FLAG-tagged ADRB2 (Figure S10A). Intracellular cAMP levels of cells overexpressing ADRB2 did not change significantly following ESYT1 KD (Figure S10B), suggesting the effect of ESYT1 on GPR133 signaling is specific to this receptor and not due to interference with Gαs function.

To rule out an interaction of ESYT1 with adenylate cyclase, we analyzed the effects of ESYT1 KD and ESYT1 overexpression on the cAMP response to forskolin (FSK), an adenylate cyclase activator, in HEK293T cells (Figures S10C and S10D). After incubation with a range of FSK concentrations (1, 5, and 10 μM), intracellular cAMP levels increased indistinguishably after either ESYT1 KD (Figure S10C) or ESYT1 overexpression (Figure S10D), suggesting the ESYT1 levels do not influence adenylate cyclase function.

Collectively, these observations suggest that ESYT1 acts to dampen GPR133 signaling. This effect is specific to GPR133 and not due to ESYT1 interference with Gαs signaling or adenylate cyclase function.

The ESYT1 C2C domain is required for its interaction with GPR133

ESYT1 has five C2 domains (C2A–E) (Figure 3A). Among these domains, C2C and C2E are required for the formation of ER-PM tethers in a Ca^{2+}-dependent manner.[21,24,26,28] The current mechanistic model posits that C2C and C2E interact at rest, but upon increases in cytosolic Ca^{2+}, C2C binds Ca^{2+} to derepress C2E attachment to phospholipids in the PM, particularly $PI(4,5)P_2$ (phosphatidylinositol (4,5)-biphosphate). HEK293 cells also transcribe *ESYT2* mRNA and express ESYT2 protein, albeit to a lesser extent than ESYT1,[34,35] but ESYT2 lacks the Ca^{2+} dependence in forming ER-PM bridges and contains only three C2 domains (Figures S11A and S11B). The C2C domain of ESYT2 is considered equivalent to the C2E domain of ESYT1, in that it mediates the attachment to phospholipids in the PM.[21,22,24,28] By the same token, the C2A and C2B domains are functionally conserved among all ESYT proteins and are thought to regulate the dimerization of the SMP domains, which mediate ER-PM lipid transfer.[24] Our proximity biotinylation discovery assay using GPR133 as bait revealed significantly higher enrichment of ESYT1 compared to ESYT2, suggesting a strong putative interaction of GPR133 with ESYT1 and a weaker interaction with ESYT2 (Table S1). Combined with what is known about the function of ESYT protein domains, our data raise the possibility that the robust GPR133-ESYT1 interaction may be mediated by C2 domains unique to ESYT1 that confer Ca^{2+} dependence in ESYT1-mediated ER-PM bridge formation. Thus, we tested whether deletion of the C2C (ΔC2C) domain of ESYT1 modulates the interaction with GPR133 (Figure 3A). We also tested whether the C2E domain, which is necessary for tethering to the PM, regulates the interaction, by deleting C2E alone (ΔC2E) or in combination with C2C (ΔC2C+E) (Figure 3A).

First, we compared the effects of all deletion mutants and full-length ESYT1 on GPR133 surface expression (Figure 3B) and signaling (Figure 3C). We transfected naive HEK293T cells or HEK293T cells stably overexpressing GPR133 with WT ESYT1, ESYT1 ΔC2C, ESYT1 ΔC2E, and ESYT1 ΔC2C+E, as well as an empty vector control. Expression of

ESYT1 constructs and GPR133 was confirmed by western blots of whole-cell lysates (Figure S12). GPR133 surface expression at the PM, as assessed by ELISA in non-permeabilized cells, did not change following overexpression of full-length ESYT1 or any of the deletion mutants (Figure 3B). However, we found that deletion of the C2C domain had a significant impact on GPR133 signaling (Figure 3C). In contrast to the robust decrease in cAMP following transfection of WT ESYT1, overexpression of ΔC2C significantly increased cAMP levels in GPR133-expressing HEK293T cells compared to the empty vector control or WT ESYT1. The ΔC2E deletion mutant was not different from full-length ESYT1. Overexpression of the double-deletion mutant ΔC2C+E had a positive effect on signaling similar to the effect of the single ΔC2C deletion mutant, albeit not as pronounced. These data suggest that deletion of the C2C domain impacts the interaction between ESYT1 and GPR133. The fact that the magnitude of the effect of the ΔC2C deletion on GPR133 signaling exceeds that of the empty vector suggests that this mutant may have dominant negative effects on endogenous ESYT1, possibly mediated by heteromultimer formation between the mutant and the endogenous proteins.[21,29]

Next, we tested whether the affinity of the interaction between GPR133 and ESYT1 was affected by deletions of C2C and C2E. We performed affinity co-purification studies, using HEK293T cells stably overexpressing WT GPR133 with a Twin-Strep-tag at the C terminus and naive HEK293T cells as control (CTRL). We transfected these cells with constructs for full-length ESYT1, ΔC2C, ΔC2E, or ΔC2C+E, or an empty vector, and pulled down Strep-tagged GPR133 using Strep-Tactin XT-coated magnetic beads. Western blots of whole-cell lysates confirmed overexpression of GPR133 and the ESYT1 constructs (Figure 3D, input). The electrophoretic mobility of ESYT1 constructs reflected their predicted sizes (WT ESYT1 ~123 kDa, ΔC2C ~109 kDa, ΔC2E ~109 kDa, and ΔC2C+E ~95 kDa). Following the Strep-Tactin-based purification, we detected GPR133 in all elution samples of cells overexpressing Strep-tagged GPR133 (Figure 3D, elution). Using an antibody against ESYT1, we detected ESYT1 bands in GPR133-expressing cells transfected with either full-length ESYT1 or ΔC2E, but not ΔC2C or ΔC2C+E (Figure 3D, elution). Collectively, the signaling and biochemical data suggest that the C2C domain of ESYT1 is essential for the interaction with GPR133.

Modulation of GPR133 signaling by ESYT1 depends on intracellular Ca^{2+}

ESYT1 forms ER-PM bridges in response to cytosolic Ca^{2+} flux.[21–24,26,28,30] C2C is the ESYT1 domain thought to be primarily responsible for the Ca^{2+}-sensor properties of ESYT1.[21,26] It was previously shown that the D724A point mutant in the C2C domain of ESYT1 renders it insensitive to Ca^{2+}, thereby preventing ESYT1-mediated ER-PM bridge formation in a Ca^{2+}-dependent manner.[26] To determine whether loss of Ca^{2+} sensing influences the ESYT1-GPR133 interaction, we generated the D724A mutant ESYT1.[26] To confirm that the D724A mutation or deletion of the C2C and C2E domains impairs the Ca^{2+}-induced PM localization of ESYT1, we performed confocal immunofluorescence microscopy in HEK293T cells stably overexpressing MAPPER, a fluorescent reporter for ER-PM junctions.[26] We transfected HEK293T-MAPPER cells with Myc-tagged WT ESYT1, the Ca^{2+}-insensitive mutant D724A, or the deletion mutants lacking the C2C domain, the C2E domain, or both C2C and C2E domains. We compared the ESYT1

localization in these cells before and after treatment with 1 μM thapsigargin (TG). TG increases intracellular Ca^{2+} levels (Figure S13) by blocking its reuptake into the ER by the ER Ca^{2+} ATPase, thereby depleting Ca^{2+} stores in the ER and promoting store-operated Ca^{2+} entry (SOCE).[36] By staining with an antibody against GFP (detecting MAPPER, green) and Myc (detecting ESYT1, red), we detected an increase in the overlap (orange) of WT, full-length ESYT1, and MAPPER following TG treatment compared to the control condition (DMSO treatment), suggesting formation of ER-PM tethers (Figures 4A and S14). However, we did not observe such overlap following TG treatment with the D724A and the deletion mutants (Figures 4A and S14). This finding suggests that translocation of ESYT1 to ER-PM bridges was prevented following the alteration of its Ca^{2+}-sensing capacity.

We then tested how increases in cytosolic Ca^{2+} brought about by TG modulate GPR133 signaling in HEK293T cells stably overexpressing GPR133 and transfected with WT ESYT1, the Ca^{2+}-insensitive mutant D724A, or a vector control. D724A ESYT1 did not affect GPR133 surface expression, but decreased basal levels of GPR133 signaling, similar to the effect following transfection of WT ESYT1 (Figures S15A and S15B). To trigger an increase in intracellular Ca^{2+}, we treated cells with 1 μM TG (Figures 4A–4G). TG had no effect on GPR133 surface expression compared to control treatment with DMSO in any of the experimental groups (Figures 4B–4D and 4F). However, cAMP levels significantly increased in response to TG in cells overexpressing GPR133 and either an empty vector or WT ESYT1 (Figure 4C). In contrast, we did not observe significant changes in cAMP levels following TG in cells transfected with the Ca^{2+}-insensitive mutant D724A (Figure 4C). To confirm that the Ca^{2+}-dependent increase in GPR133 signaling is mediated by ESYT1, we repeated the TG treatment in HEK293T cells overexpressing GPR133 and transduced with lentiviral shSCR or shESYT1. GPR133 surface expression in ELISAs was not affected by TG in either condition (Figure 4D). While we observed significantly increased cAMP levels following the treatment of HEK293T cells expressing GPR133 and shSCR with TG compared to the DMSO control (Figure 4E), the TG treatment had no effect on GPR133 signaling following ESYT1 KD (Figure 4E). In agreement with our previous observations, we did not detect significant changes in GPR133 surface expression (Figure 4F) or TG modulation of GPR133-driven cAMP levels following overexpression of the Ca^{2+}-insensitive deletion mutants ΔC2C, ΔC2E, or ΔC2C+E (Figure 4G).

These findings raise the possibility that ESYT1, which normally acts to dampen GPR133 signaling via an interaction mediated by its C2C domain, may dissociate from GPR133 when intracellular Ca^{2+} concentration rises, as occurs after TG treatment. To test this hypothesis, we performed an ESYT1-GPR133 proximity ligation assay (PLA) (Figure 5). We transfected HEK293T cells with GPR133 alone or together with Myc-tagged ESYT1 (Figure 5A). Using confocal immunofluorescence microscopy, we detected cells overexpressing GPR133 (green) or ESYT1 (red), with most transfected cells expressing both proteins (orange arrows) (Figure 5A). Western blots of whole-cell lysates further confirmed overexpression of ESYT1 and GPR133 (Figure 5B). We then performed the PLA using an anti-GPR133 (rabbit) antibody and an anti-Myc antibody (mouse) on cells transfected with either GPR133 alone or both GPR133 and ESYT1 (Figure 5C). The PLA signal (red) was detected only in cells co-transfected with both GPR133 and ESYT1. Most importantly, the PLA signal weakened in cells overexpressing GPR133 and ESYT1 after treatment with TG

compared to DMSO (Figure 5D). Optical sections from the imaged areas confirmed these observations (Figure 5E). These findings support the hypothesis that the ESYT1-GPR133 interaction is weakened when intracellular Ca^{2+} increases.

Collectively, our data suggest that ESYT1 binds GPR133, an interaction dependent on the C2C domain of ESYT1, until cytosolic Ca^{2+} increases release ESYT1 from GPR133, thus derepressing GPR133 signaling.

ESYT1 KD increases GPR133 signaling GSCs

We have previously shown that GPR133 is expressed *de novo* in GBM relative to normal brain tissue and is necessary for GBM growth.[14,15] We, therefore, investigated whether the effects of ESYT1 on GPR133 signaling in HEK293T cells are reproducible in patient-derived GSCs. First, we tested whether endogenous ESYT1 co-purifies with exogenous overexpressed WT GPR133 tagged at the C terminus with Twin-Strep in a patient-derived GSC culture (GBML128). Similar to our findings in HEK293T cells, we found enrichment of ESYT1 after purification of the tagged CTF of GPR133 (Figure 6A).

We then transduced patient-derived GSCs (GBML109) with lentiviral GPR133 overexpression and shESYT1 constructs. Endogenous ESYT1 protein levels were reduced following transduction with lentiviral shESYT1 compared to shSCR, as shown by western blot (Figures 6B and S16). Similar to HEK293T cells, cAMP levels significantly increased in GBML109 following ESYT1 KD compared to control (shSCR) (Figure 6C). This finding demonstrated the impact of ESYT1 KD on GPR133 signaling in different cell types and pointed out its potential relevance in a disease-related biological context.

Effects of ESYT1 KD on tumor growth

The role of ESYT1 in GBM has not been studied so far. We hypothesized that, if ESYT1's principal action in GBM is to dampen GPR133 signaling, ESYT1 KD or KO should produce an increase in tumorsphere formation. However, we also anticipated that ESYT1 is likely to have additional functions in GBM, which could influence the outcome of the tumorsphere assay beyond its action on GPR133 signaling.

To determine the pattern of *ESYT1* expression in GBM, we used single-cell RNA-sequencing (scRNA-seq) data of adult and pediatric GBM from the Single Cell Portal of the Broad Institute (Figure S17A, i). Indeed, *ESYT1* is transcribed in a significant portion of GBM cells, as well as other cell types, in the tumor microenvironment (Figure S17A, ii). When we analyzed patient survival data as a function of *ESYT1* mRNA levels on bulk RNA-seq from surgical specimens in the GBM dataset of the TCGA (The Cancer Genome Atlas), we found that elevated *ESYT1* expression levels inversely correlate with survival (Figure 6D). Using data from the TCGA, CGGA (Chinese Glioma Genome Atlas), and Rembrandt databases, we found that *ESYT1* is found throughout the glioma family, but its expression is highest in histologic grade IV and *IDH* (isocitrate dehydrogenase) WT tumors, which represent GBM (Figures S17B and S17C). These findings raised the possibility that increased *ESYT1* expression may correlate with more aggressive tumor behavior.

To gain more insight into the function of ESYT1 in tumor biology, we first investigated how *ESYT1* expression is regulated, comparing undifferentiated GSCs maintained in medium with EGF/bFGF to differentiated GBM cells (DGCs) cultured in serum. ESYT1 transcripts decreased after differentiation in one of three patient-derived cultures tested, but remained unchanged in the other two (Figure S18A). This finding suggested that ESYT1 is present in both stem-like and differentiated lineages in GBM tumors.

We then tested whether KD or KO of ESYT1 in GSCs affects clonogenic tumorsphere formation *in vitro.*[14] Such assays are a measure of the potential of single tumor cells to initiate growth and are considered a metric of the frequency of GSCs *in vitro*. First, we knocked down ESYT1 in the patient-derived GBM culture GBML154 (Figures 6E and 6F), using the same approach as in HEK293T cells and GBML109. Western blots of whole-cell lysates confirmed expression of ESYT1 and its KD (Figure 6E). We then seeded single-cell suspensions of GBML154 cells transduced with shSCR or shESYT1 and counted tumorspheres that formed after 2 weeks (Figure 6F). The number of tumor-spheres was significantly reduced in GBML154 after ESYT1 KD compared to control (Figure 6F). In a parallel experiment, we designed CRISPR-Cas9-mediated KO of ESYT1 in three different patient-derived GBM cultures (GBML83, GBML137, and GBML154), using the same approach as in HEK293T cells. Reduction in ESYT1 protein levels was demonstrated with western blot (Figure 6G). In agreement with our findings following KD of ESYT1 in GSCs, extreme limiting dilution assays (ELDAs) showed that ESYT1 KO reduced clonogenic tumorsphere formation in all GBM cultures, compared to a *Rosa26*-targeting gRNA control (Figures 6H and 6I). To show the specificity of the ESYT1-KO approach, we transduced the ESYT1-KO GBM cells with lentiviral ESYT1 overexpression constructs. Indeed, the impairment in tumorsphere formation in ESYT1-KO cells was rescued following overexpression of exogenous ESYT1 (Figure 6H). This finding demonstrated the specificity of the phenotype induced by the KO of ESYT1.

Finally, we tested the impact of ESYT1 KO on tumor initiation *in vivo* using orthotopic xenograft implantation of GBML137 GSCs in immunodeficient NSG mice (Figures S18B and S18C). Longitudinal IVIS imaging indicated a trend toward slower tumor growth in the ESYT1-KO condition relative to *Rosa26* controls, which did not reach statistical significance. In summary, our experiments with GSCs suggest that ESYT1 may have some pro-tumorigenic functions in GBM that extend beyond its interaction with GPR133. Alternatively, our findings may indicate that tumor growth may depend on the pulsatile character of GPR133 signaling conferred by its regulation by ESYT1 and Ca^{2+}, while tonic GPR133 signaling in the absence of ESYT1 may be harmful to GBM cells.

DISCUSSION

GPR133 is an aGPCR that signals through Gαs to raise cAMP, with an essential role in GBM growth.[8,9,14,17–20] Previous work by us and others has demonstrated that autoproteolytic cleavage at the GPS and NTF-CTF dissociation promote receptor signaling, but are not absolutely necessary for receptor activation.[8,17–19] Furthermore, although ligand binding to the extracellular portion of GPR133 increases its signaling output, the receptor maintains high basal levels of activity even in the absence of ligands.[8,17–20] These facts

raise the question of how cells may regulate the intrinsic signaling capacity of GPR133. Here, we have uncovered an interaction between GPR133 and ESYT1, an ER-anchored protein that forms ER-PM tethers via C2 domains in response to increases in cytosolic Ca^{2+}.[21–29] ESYT1 belongs to a family of three extended synaptotagmins (ESYT1–3), which all carry out the same function of tethering the ER to the PM and, by doing so, possibly mediate the exchange of phospholipids between the ER and the PM lipid bilayers. However, ESYT1's ability to form ER-PM tethers depends significantly more on Ca^{2+} than ESYT2 and ESYT3.[21] Although our data cannot ascertain direct binding of ESYT1 to GPR133, we have collected compelling evidence that the two proteins at least reside in close proximity, which allows for regulation of GPR133 signaling by ESYT1.

While ESYT1 and ESYT2 are both expressed in HEK293T cells,[34,35] in which we performed the proximity biotinylation discovery assay, ESYT1 is the predominant species. Accordingly, our proteomic analysis indicated a significantly more abundant interaction between GPR133 and ESYT1 relative to ESYT2, suggesting that the Ca^{2+} dependence of ESYT1 may be critical in the regulation of GPR133 signaling. Indeed, the GPR133-ESYT1 interaction depends on one of the C2 domains of ESYT1, C2C, which was previously shown to be necessary for the Ca^{2+}-dependent ER-PM tethering function of ESYT1.[21,23,25,28] At baseline Ca^{2+} concentrations, ESYT1 acts to suppress signaling by GPR133. However, increases in cytosolic Ca^{2+} lead to dissociation of ESYT1 from GPR133 and derepression of GPR133 signaling. This action of Ca^{2+} on GPR133 signaling is specifically mediated by ESYT1, because it is abolished when ESYT1 is knocked down or is rendered Ca^{2+} insensitive by deletion of the Ca^{2+}-sensing C2 domains or the D724A point mutation in its C2C domain.

ESYT1 was previously shown to mediate PM trafficking of certain membrane proteins, such as ANO1.[37] While GPR133 is also subject to trafficking from the ER to the PM through the secretory pathway,[8] the signaling-suppressive actions of ESYT1 on GPR133 do not seem to regulate its trafficking or alter its PM localization, regardless of cytosolic Ca^{2+} levels. Several different explanations can be considered for this observation. First, it is possible that much of the GPR133 basal signaling output occurs while the receptor is being trafficked through the secretory pathway to the PM, but does not require PM localization. Second, ESYT1 may interact with PM-localized GPR133 as one component of a dynamic equilibrium that also includes the ESYT1-PM interactions, with elevations in cytosolic Ca^{2+} shifting the equilibrium to favor ESYT1-GPR133 dissociation and ESYT1-PM tethering. Finally, our ability to detect subtle changes in PM levels of GPR133 as a result of perturbation of ESYT1 levels may be technically limited.

The mechanism underlying the suppression of GPR133 signaling by ESYT1 remains unclear. GPR133 manifests elevated basal levels of Gαs-cAMP signaling, even in heterologous expression systems, such HEK293 cells, and in the absence of known ligands. This raises the possibility of baseline avid interactions with the G-protein machinery. Our working hypothesis is that ESYT1 competes with G proteins for GPR133 binding. In this model, cytosolic Ca^{2+} flux derepresses signaling by reducing ESYT1 affinity for GPR133 and allowing G-protein interactions with the receptor. Relevant to this hypothesis is the finding that G-protein subunits are detected in our proximity biotinylation discovery assay

(Tables S2 and S1). The fact that ESYT1 is found in the proximity of both WT and the signaling-hypomorph mutant GPR133 indicates a “structural” rather than a signaling-dependent ESYT1-GPR133 interaction. In other words, we hypothesize that the structural interactions of GPR133 with ESYT1 do not depend on receptor cleavage or the potency of the endogenous orthosteric agonist Stachel sequence and the signaling capacity of the receptor. Future experiments will be needed to determine whether ESYT1 indeed competes with G proteins for GPR133 binding.

The GPR133-ESYT1 interaction is dynamically regulated by Ca^{2+}. Increases in cytosolic Ca^{2+} lead to dissociation of ESYT1 from GPR133 on PLAs and derepression of GPR133 signaling. This modulation represents an example of crosstalk between two dominant signaling pathways in cells: Ca^{2+} and cAMP. This mechanism may be particularly relevant in GBM, where several groups have demonstrated robust cytosolic Ca^{2+} waves in tumor cells, which promote tumor growth.[38–41] We postulate that such waves boost GPR133 signaling in GBM cells by causing dissociation of ESYT1 from GPR133, a mechanism that may mediate some of the tumor-promoting effects of Ca^{2+} waves and will require further testing. Interestingly, KD or KO of ESYT1 in GBM reduces tumor growth *in vitro* and *in vivo* to a lesser extent, suggesting either that ESYT1 has multiple functions in these tumors that extend beyond its interaction with GPR133 or that constitutive cAMP signaling by GPR133 in the absence of ESYT1 is not tolerated by tumor cells. In the latter hypothetical scenario, we speculate that ESYT1- and Ca^{2+}-regulated pulsatile GPR133 signaling is fine-tuned to support tumorigenic processes.

Of particular interest is the possibility that the ESYT1-GPR133 interaction may exert bidirectional effects on the functions of both proteins. Our work has uncovered effects of this interaction on GPR133 signaling, but potential regulation of ESYT1 biology by GPR133 will require future investigation. ESYT1 is thought to mediate lipid transfer between the ER and the PM in a Ca^{2+}-dependent manner.[21,22,24–26,28,29] This action not only may be relevant to lipid metabolism, but may also help regulate signaling cascades. As an example, activation of phospholipase C (PLC) by cell-surface receptors leads to hydrolysis of PI(4,5) P_2, the PM phospholipid that the C2E domain of ESYT1 has high affinity for, to generate the second messengers inositol triphosphate (IP_3) and diacylglycerol (DAG). The former gates IP_3 receptors on the ER to release Ca^{2+} from ER stores into the cytosol, while the latter activates protein kinase C (PKC). Among the proposed functions of ESYT1 is the recycling of DAG from the PM to the ER, thereby potentially attenuating PKC signaling and modulating other DAG-dependent cellular processes.[42] Furthermore, ESYT1 has been implicated in the regulation of SOCE.[30] It is, therefore, plausible that GPR133 may play a regulatory role in these processes via its interaction with ESYT1.

Collectively, our findings link cytosolic Ca^{2+} flux, which is a potent modulator of several signaling cascades and cellular processes, to regulation of Gαs-cAMP signaling by GPR133 via a mechanism mediated by the GPR133-ESYT1 interaction. We postulate that the GPR133-ESYT1 interaction will serve as a paradigm for exploring similar mechanisms that modulate signaling by other aGPCRs. We theorize that this interaction may be biologically relevant to the pathogenesis of GBM, a brain malignancy in which both cytosolic Ca^{2+} waves and GPR133 are essential to tumor growth. Finally, our proximity biotinylation

proteomic database serves as a resource for future investigation of both “structural,” signaling-agnostic, and signaling-dependent intracellular interactors of GPR133.

Limitations of the study

One limitation of the study relates to the lack of certainty regarding the role of ESYT1 in GBM. Our functional assays in patient-derived GBM cultures indicated a primarily tumorigenic role for ESYT1. Interpretational caveats in our GBM experiments are that our *in vivo* tumor initiation assay showed only a trend, and not a definitive effect, of ESYT1 KO to slow tumor growth, and *ESYT1* expression is preserved not only in GSCs but also in DGCs in two of three tested GBM cultures, suggesting it may not regulate solely stem-like phenotypes, but also other aspects of tumor biology in GBM.

Reconciling the predominantly pro-tumorigenic function of ESYT1 in GBM with our working hypothesis as to the role of GPR133 is challenging. In principle, if ESYT1 function pertained solely to regulation of GPR133 signaling, then, given the known oncogenic function of GPR133 in GBM, we would expect it to act as a tumor suppressor. However, a reasonable prediction is that ESYT1 carries out other functions beyond its interaction with GPR133. It is also possible that tonic GPR133 signaling in the absence of ESYT1 does not serve the same tumorigenic function that pulsatile signaling does in the presence of Ca^{2+} waves and ESYT1. Instead, we speculate that the Ca^{2+} dependence of the regulatory effects of ESYT1 on GPR133 signaling confers a pulsatile nature to the cAMP signal produced by GPR133, which temporally correlates with Ca^{2+} waves in GBM cells and supports tumorigenic processes. Future studies will be required to further clarify these questions.

An additional limitation of the study is that the discovery assay was performed in HEK293T cells and not patient-derived GBM cultures. This approach was preferred for technical reasons, but we admit it may not have accurately captured the intracellular interactome of GPR133 in the context of GBM. Nonetheless, we were able to validate the GPR133-ESYT1 interaction and its functional consequences in patient-derived GBM cells.

Finally, our proximity biotinylation discovery approach identifies proteins in proximity to GPR133 throughout its trafficking from the ER to the cell surface and is not specific to interactors at the PM. We, therefore, caution the reader that the current experiments do not prove that the described modulation of GPR133 signaling by ESYT1 occurs at the PM. It is possible that this interaction may exert its effects anywhere along the trafficking of GPR133 from the ER to the PM.

STAR★METHODS

RESOURCE AVAILABILITY

Lead contact—Further information and requests for resources and reagents should be directed to and will be fulfilled by the lead contact, Dimitris Placantonakis (dimitris.placantonakis@nyulangone.org).

Materials availability

- Expression plasmids generated in this study (detailed in the Key Resources table) will be available upon request.

Data and code availability

- Proteomic data generated by this study have been deposited at MassIVE (UCSD, https://massive.ucsd.edu/ProteoSAFe/static/massive.jsp) under accession number MSV000091163.
- This paper does not report original code.
- Any additional information required to reanalyze the data reported in this paper is available from the lead contact upon request.

EXPERIMENTAL MODEL AND SUBJECT PARTICIPANT DETAILS

Cell culture—Human embryonic kidney 293 T cells (HEK293T, Takara, Cat# 632180) were cultured in Dulbecco's modified Eagle's medium (DMEM, Gibco, Cat# 11965–118) with sodium pyruvate (Gibco, Cat# 11360070) and 10% fetal bovine serum (FBS; Peak Serum, Cat# PS-FB2) at 37 °C and 5% CO_2. Patient-derived GBM cultures were established as previously described[44]. GBM cells were cultured in Neurobasal medium (Gibco, Cat# 21103049) supplemented with N2 (Gibco, Cat# 17-502-049), B27 (Gibco, Cat# 12587010), non-essential amino acids (Gibco, Cat# 11140050) and GlutaMax (Gibco, Cat# 35050061), as well as 20 ng/mL recombinant basic Fibroblast Growth Factor (bFGF; R&D, Cat# 233-FB-01M) and 20 ng/mL Epidermal Growth Factor (EGF; R&D, Cat# 236-EG-01M) at 37°C, 5% CO_2 and 4% O_2. Patient-derived GSCs were grown in spheroid suspensions, or as attached cultures on cell culture dishes pretreated with poly-L-ornithine (Sigma, Cat# P4957) and laminin (Thermo Fisher, Cat# 23017015). HEK293T cells were passaged using Trypsin (Thermo Fisher, Cat# 25300054) and GSCs were dissociated and passaged with Accutase (Innovative Cell Technologies, Cat# AT104).

***In vivo* GBM xenografts—**Mice were housed within NYU Langone Medical Center's Animal Facilities. All animal procedures were performed according to an IACUC-approved protocol. Orthotopic intracranial xenografts have been described in detail previously[45]. In short, immunodeficient NSG (NOD.Cg-*Prkdc*^{scid} *Il2rg*^{tm1Wjl}/SzJ) mice (6–8 weeks of age) were anesthetized with intraperitoneal injection of ketamine/xylazine (10 mg/kg and 100 mg/kg, respectively). A midline skin incision was made and a small hole was drilled through the skull 2 mm off the midline and 2 mm anterior to the coronal suture. Mice were then stereotactically injected with 2×10^5 GBM cells lentivirally infected with a luciferase-containing plasmid. The skin incision was sutured and animals were closely monitored during the recovery period.

METHOD DETAILS

Generation of GPR133 and ESYT1 constructs—All constructs used for expression of GPR133, ESYT1 and ADRB2 or knockdown/knockout of ESYT1 are listed in Key Resources. Primers for mutagenesis, Gibson cloning and PCR are also listed in

Key Resources. Fusion constructs of WT GPR133-BioID2 and mutant GPR133 (H543R/T545A)-BioID2 were created using the MCS-13X Linker-BioID2-HA (Addgene #80899) [31] plasmid and subsequently subcloned into the lentiviral backbone pLVX-EF1a-mCherry-N1 (Takara, Cat# 631986). TwinStrep-tagged GPR133 constructs were available from previous studies[8]. ESYT1, ADRB2 and MAPPER cDNA plasmids were obtained from Addgene (Myc-ESYT1 #66833, EFGP-ESYT1 #66830, Flag-ADBR2 #14697, GFP-MAPPER #117721). Plasmids expressing Myc-tagged cDNAs encoding other candidate interactors (OXSR1, CYFIP2, NAE1, RHOT2) were obtained from Sino Biological and Addgene. The D724A point mutant from ESYT1 was generated by site-directed mutagenesis using the Q5® Site-Directed Mutagenesis Kit (NEB, Cat# E0554S), following the manufacturer's protocol. ESYT1 deletion mutants ΔC2C, ΔC2E and ΔC2C+E were created from the full-length ESYT1 sequence using a two-fragment Gibson reaction.

Transfection and lentiviral infection—HEK293T cells were transfected with plasmid DNA using Lipofectamine 2000 (Invitrogen, Cat# 11668–019), following the manufacturer's protocol. Selection of HEK293T cells stably transfected with ESYT1-GFP was performed with G418 (ThermoFisher, Cat# 10131035). HEK293T or GBM cells were transduced using lentivirus as described previously[46]. In short, lentivirus was produced by co-transfecting HEK293T cells with expression plasmids of interest and packaging plasmids psPax2 and pMD2.G. Lentivirus was collected from the cell culture supernatant 24h, 48h, and 72h after transfection and concentrated using the Lenti-X concentrator (Contech Takara, Cat# 631231). For lentiviral transduction, HEK293T or GBM media was supplemented with 4 μg/ml protamine sulfate and cells were treated with viral particles at a multiplicity of infection (MOI) of three. Stable cell lines were selected with 5 μg/mL puromycin and/or by isolating mCherry- or GFP-positive cells by fluorescence-activated cell sorting (FACS) with the SH800Z sorter (Sony Biotechnology).

Western blot analysis of whole cell lysates—Cells were washed with PBS and lysed in RIPA buffer (Thermo, Cat#89900) containing Halt protease inhibitor cocktail (Thermo, Cat# 78429) and 1% n-dodecyl β-D-maltoside (DDM) (Thermo, Cat# BN2005). Lysates were sonicated in a water-bath Bioruptor (Diagenode, Cat# UCD-300) and precleared at 15,000 x g for 10 min at 4 °C. Protein concentrations were measured using the DC protein assay kit II (BioRad, Cat# 5000112). Laemmli buffer (BioRad, Cat# 1610747) containing DTT (BioRad, Cat# 1610610) was then added and samples were incubated at 37 °C for 30 min. Twenty μg of protein samples were separated by SDS-PAGE and transferred to nitrocellulose membranes (BioRad, Cat# 1620112). Membranes were blocked in 2% bovine serum albumin (BSA) in TBS-Tween for 1 hour at room temperature (RT), incubated with primary antibodies at 4 °C overnight, washed with TBS-Tween and incubated with Alexa Fluor or HRP-conjugated secondary antibodies for 1 hour at RT. Images were acquired using the iBrightFL1000 system (Invitrogen). Signals were detected by fluorescence or chemiluminescence (Thermo Scientific, Cat# 34577). Densitometric analysis of band intensities was done using ImageJ.

Identification of intracellular interaction partners by proximity biotinylation / nano-liquid chromatography coupled to tandem mass spectrometry (nanoLC-MS/MS)

Sample processing: HEK293T cells were transduced with lentivirus to stably overexpress WT GPR133-BioID2, mutant (H543R/T545A) GPR133-BioID2 or an empty vector control. Cells were treated with 50 μM biotin (Sigma, Cat# B4639–500MG) for 16 hours and whole cell lysates were prepared as described above. Biotinylated proteins were isolated using Pierce™ NeutrAvidin™ Agarose beads (Thermo Fisher, Cat# 29200) following the manufacturer's protocol. Affinity-enriched proteins were separated by SDS-PAGE until the dye front entered 3 cm into the separating gel, and resulting gels were washed 3 times in distilled deionized H_2O for 15 minutes each and visualized by staining overnight with EZ-Run Protein Gel Staining Solution (Thermo Fisher Scientific, Cat# BP36201). Stained protein gel regions were typically excised into 4 gel sections per gel lane, and destained as described [47]. In-gel digestion was performed overnight with MS-grade trypsin (Trypsin Gold, Promega, Cat# V5280) at 5 ng/μL in 50 mM NH_4HCO_3 digestion buffer. After acidification with 10% formic acid (final concentration of 0.5–1% formic acid), resulting peptides were desalted using hand-packed, reversed phase Empore C18 Extraction Disks (3M, Cat#3M2215), following an established method [48]. Each of the 4 sections per sample, per gel lane, were excised and separately digested in-gel, at the same time, using the same batch and amount of trypsin. The peptides from each of these gel sections were purified and analyzed by nano-LC-MS/MS separately. After MS, MaxQuant data analysis was performed by merging the 4 MS files for each sample, as one Experiment under "Set Experiment" tab.

MS data acquisition: Desalted peptides were concentrated to a very small droplet by vacuum centrifugation and reconstituted in 10 μL 0.1% formic acid in H_2O. Approximately 90% of the peptides were analyzed by nano-LC-MS/MS). A Q Exactive HF mass spectrometer was coupled directly to an EASY-nLC 1000 (Thermo Fisher Scientific, Cat#LC120) equipped with a self-packed 75 μm x 20-cm reverse phase column (ReproSil-Pur C18, 3M, Dr. Maisch GmbH, Germany) for peptide separation. Analytical column temperature was maintained at 50 °C by a column oven (Sonation GmBH, Germany). Peptides were eluted with a 3–40% acetonitrile gradient over 60 min at a flow rate of 250 nL/min. The mass spectrometer was operated in DDA mode with survey scans acquired at a resolution of 120,000 (at m/z 200) over a scan range of 300–1750 m/z. Up to 15 of the most abundant precursors from the survey scan were selected with an isolation window of 1.6 Th for fragmentation by higher-energy collisional dissociation with normalized collision energy (NCE) of 27. The maximum injection time for the survey and MS/MS scans was 60 ms and the ion target value (Automatic Gain Control) for both scan modes was set to $3e^6$.

MS data processing: The MS files were processed using the MaxQuant proteomics data analysis workflow (version 1.5.7.0) with the Andromeda search engine[49,50] used to search a human proteome database (Uniprot fasta, dated 122017, with 20,244 protein entries) and a file containing contaminants, such as human keratins. Trypsin digestion was specified allowing up to 2 missed cleavages with the minimum required peptide length set to be seven amino acids. N-acetylation of protein N-termini, oxidation of methionines and deamidation of asparagines were set as variable modifications. For the initial identification search,

parent peptide masses were allowed mass deviation of up to 20 ppm. Peptide spectral matches and protein identifications were filtered using a target-decoy approach at a false discovery rate of 1%. We used the raw MS1 intensity for protein quantification without the match-between-runs feature. Briefly, maximum MS intensities for each peptide over the chromatographic run (MS1 RAW intensity) were extracted. These peptide intensities were normalized between samples for each individual corresponding gel fraction (measured in separate LC-MS experiments) and peptide normalization was carried forward ("delayed normalization") during subsequent protein level quantification analyses. Proteins were quantified pair-wise based on individual peptide ratios (unique and razor peptides) for each protein group. Details of peptide and protein level quantification and normalization by the MaxLFQ software (Maxquant version 1.5.7.0) are as previously described[50,51].

Computational analysis of biotinylated interaction partners—All intensity values obtained from MaxQuant were transformed as $\log_{10}$ (raw intensity +1). Zero values were imputed by the smallest non-zero value in the entire empirical distribution of all 9 samples and 1379 proteins. Differential analysis was performed between WT (n=3) vs. empty vector (PuroR, n=3), mutant (H543R/T545A, n=3) vs. empty vector, and mutant vs. WT groups, using the R package limma. To identify significant interactors for WT and mutant GPR133 relative to control (PuroR), we set criteria of positive mean $\log_{10}$ fold change of the WT-PuroR and mutant-PuroR comparisons >1, and p value$<10^{-5}$ ($-\log_{10}$ p value>5) (Table S2). To determine differentially biotinylated interactors between the WT and mutant conditions, all proteins were ranked by the p value of the mutant vs. WT comparison, and a threshold was set at p value$<10^{-5}$ and $\log_{10}$ fold change>1 (Table S3). Among those, a secondary filter was used to identify those proteins that also met criteria as significant interactors for either WT or mutant GPR133 in the comparison to the PuroR control condition. Gene Set Enrichment Analysis (GSEA) was performed with the R package fgsea, with the canonical pathway gene sets collection (c2.cp v7.0) as the search source in MSigDB. The raw mass spectrometry data and accompanying tables generated in this study are available at MassIVE (UCSD, https://massive.ucsd.edu/ProteoSAFe/static/massive.jsp) under accession number MSV000091163.

Affinity purification of Strep-tagged GPR133 and co-purification of ESYT1—For input samples, whole cell lysates were prepared as described above. TwinStrep-tagged GPR133 was purified using Strep-Tactin® XT coated magnetic beads (MagStrep "type3" XT Beads, IBA, Cat# 2-4090-002), according to the manufacturer's protocol. In brief, after adding Biolock (IBA, Cat# 2-0205-250), whole cell lysates were incubated with MagStrep "type3" XT Beads overnight at 4°C. The next day, beads were collected with a magnetic separator and washed 3 times with 1x Buffer W (IBA, Cat# 2-1003-100). Proteins were eluted with 1X biotin elution buffer BXT (IBA, Cat# 2-1042-025). Laemmli buffer with DTT was added and elution samples were analyzed by Western blot as described above. Membranes were stained with a rabbit antibody specifically recognizing the cytosolic aspect of GPR133 (Sigma, Cat# HPA042395) or a rabbit antibody against ESYT1 (Sigma, Cat# HPA016858), and a goat-anti GAPDH antibody (Thermo Firsher, Cat# PA1–9046) as loading control for each membrane. In experiments screening other putative interactors

(OXSR1, CYFIP2, NAE1, RHOT2), a crosslinking step with the cell membrane-permeant agent DSS (Thermo Fisher) was included prior to cell lysis and purification.

Immunofluorescent staining—For immunofluorescent staining, cells were cultured on dishes coated with poly-L-ornithine and laminin, as described above, fixed with 4% paraformaldehyde (PFA, Sigma, Cat# P6148) for 20 min at RT, and blocked with 10% BSA in phosphate-buffered saline (PBS) for 1 hour at RT. Cells were then incubated with a primary antibody in 1% BSA in PBS at 4 °C overnight. The next day, cells were washed with PBS and stained with a secondary antibody for 1 hour at RT. Nuclei were stained with 500 ng/mL 4′,6-diamidino-2-phenylindole (DAPI) or Hoechst 333442 for 10 min at RT. For permeabilized staining, 0.1% Triton X-100 was added to the BSA- or PBS solution. For experiments involving intracellular Ca^{2+} increases, cells were treated with 1 μM thapsigargin (TG) (Millipore Sigma CAS 67526-95-8) or DMSO in DMEM for 2 min or 30 min at 37°C prior to fixation. Microscopy was conducted on a Zeiss Axiovert epifluorescent microscope or a Zeiss LSM700 laser scanning confocal microscope. Co-localization of ESYT1 and MAPPER following TG treatment was analyzed using the Zen 2011 microscopy software (Carl Zeiss Microscopy).

Non-permeabilized enzyme-linked immunosorbent assay (ELISA)—Cells were seeded onto 96-well plates coated with poly-L-ornithine and laminin, as described above. Twenty-four hours after seeding, cells were washed once with cold HBSS $+Ca^{2+}/+Mg^{2+}$ (Thermo Fisher, Cat# 14025092), fixed with 4% PFA for 20 min at RT, washed three times with PBS (Gibco, Cat# 14190–250) and blocked with DMEM containing 10% FBS for one hour at RT. Cells were then incubated with 8E3E8, a monoclonal mouse antibody specifically binding the N terminus of GPR133[8,16,17], in DMEM containing 10% FBS. Cells were washed three times with PBS and incubated with horseradish peroxidase (HRP)-conjugated secondary antibodies (1:1000, chicken-anti mouse IgG Invitrogen Cat# A15975) in DMEM containing 10% FBS for 1 hour at RT. After three additional washes with PBS, cells were incubated with TMB (3,3′, 5,5′-tetramethylbenzidine)-stabilized chromogen (Thermo Fisher, Cat# SB02) for 5–10 min. The reaction was stopped by adding an equal volume of acidic stop solution (Thermo Fisher, Cat# SS04) and optical density/absorbance was measured at 450 nm ($A_{450\ nm}$).

Homogeneous time resolved fluorescence (HTRF)-based cAMP assays—HEK293T or GBM cells were seeded onto 96-well plates, pretreated with poly-L-ornithine and laminin, at a density of 75,000 cells (HEK293T) or 100,000 cells (GBM) per well. Twenty-four hours after seeding, cell culture medium, supplemented with 1 mM 3-isobutyl-1-methylxanthine (IBMX, Sigma-Aldrich, Cat# I7018–100MG) was added and cells were incubated at 37 °C for 30 – 60 min. In experiments involving elevated intracellular Ca^{2+}, 1μM TG or DMSO were added to DMEM in addition to IBMX, also for a 30 min incubation at 37°C. Concentrations of cAMP were measured using the cAMP Gs dynamic kit (CisBio, Cat# 62AM4PEC), according to the manufacturer's protocol.

Genotyping ESYT1 knockout—Genomic DNA was harvested from HEK293T cells using the DNeasy Blood & Tissue Kit (Qiagen, Cat# 69504). The portion of the *ESYT1*

gene targeted by the gRNA (exon 4) was PCR-amplified and subjected to Sanger sequencing, using the reverse primer of the PCR reaction as primer. Decomposition of sequencing aberrations was performed with TIDE[33].

Fluorescent Ca^{2+} imaging—HEK293T cells were transduced with a lentiviral vector expressing the genetically encoded Ca^{2+} indicator GCaMP6s and the fluorescent protein TdTomato[52,53]. They were imaged for 20–30 minutes on an Olympus IX73 epifluorescent microscope equipped with a SCMOS camera. Imaging data were analyzed on Olympus software.

Proximity ligation assays—For proximity ligation assays (PLA), cells were fixed, blocked and treated with primary antibodies from two different species (rabbit and mouse) at 4°C overnight, as described above. To detect proteins in close proximity, cells were then treated with PLUS and MINUS probes (Duolink® *In Situ* PLA® Probe Anti-Rabbit PLUS, Sigma, Cat# DUO92002 and Duolink® *In Situ* PLA® Probe Anti-Mouse MINUS, Sigma, Cat#DUO92004) followed by ligation and amplification steps, according to the manufacturer's protocol (Duolink® *In Situ* Detection Reagents Red, Sigma, DUO92008). Microscopy was conducted on a Zeiss LSM700 laser scanning confocal microscope. To quantify PLA signals, a total of 2 – 5 fields were acquired in each experimental condition and PLA-positive spots were counted in relation to DAPI-positive cells. Fields were averaged for each biological replicate.

Tumorsphere formation assays—Patient-derived GBM cultures were cultured as described above. Cultures were dissociated into single cells and plated at 500 cells per well in a 96-well plate. Each experimental condition was carried out in 10 technical replicate wells. Cells were grown and supplemented with fresh media and growth factors for two weeks. Individual wells of 96-well plates were imaged using automated tile scanning on an EVOS imaging system (Thermo Fisher Scientific). Tile scans of each well were exported, and sphere numbers were counted using ImageJ.

Extreme limiting dilution assays—Patient-derived GBM cells were seeded into 96-well plates with 10 replicates at each seeding density. The number of wells with spheres was recorded 14 days later. Data were visualized and statistically tested using online software (http://bioinf.wehi.edu.au/software/elda/).

Differentiation of GSCs—Differentiated GBM cells (DGCs) were derived from GBM stem cells (GSCs) by adding 10% FBS (Peak Serum, Cat# PS-FB2) to DMEM medium, in the absence of EGF and bFGF, for one week.

RNA isolation and qRT-PCR—GBM cells were lysed with Trizol (Invitrogen, Cat#15596026) and RNA was extracted with Direct-zol RNA Microprep kit (Zymo Research, Cat# R2062), according to the manufacturer's protocol. cDNA was synthesized using the iScript™ cDNA Synthesis Kit (BioRad, Cat# 1708891). Relative cDNA was quantified by performing qRT-PCR with SYBR Green PCR Master Mix (Life Technologies, A25778). qRT-PCR primers for target genes and housekeeping controls are listed in Key Resources.

IVIS imaging of GBM xenografts—*In vivo* GBM xenografts were monitored using an IVIS Lumina XR (PerkinElmer) as described previously[54]. First, mice were weighed and injected intraperitoneally with 10 μL/g body weight Luciferin substrate solution [D-Luciferin Potassium Salt (LUCK-300, Gold Biotechnology) diluted in Dulbecco's PBS (DPBS) to a final concentration of 20 mg/mL]. Mice were anesthetized using isoflurane and inserted into the IVIS imaging system. Thirteen minutes after Luciferin injection, mice were imaged at a 150 second exposure time. Living Image software (PerkinElmer) was used to quantify the "Radiance (Photons)" within the selected ROI.

Visualization of RNA-seq data—RNA-seq data from HEK293 cells were downloaded from a previous publication[34]. The data were visualized on IGV (Integrative Genomics Viewer; https://igv.org/).

Analysis of TCGA, CGGA and Rembrandt data—The normalized count reads from the pre-processed RNA-seq and microarray data (sequence alignment and transcript abundance estimation) were $\log_2$ transformed after adding a 0.5 pseudocount, to avoid infinite values upon log transformation. The GlioVis data portal was used for visualization and analysis of the datasets[43]. Statistical significance was assessed with GraphPad Prism (version 8.4.3).

QUANTIFICATION AND STATISTICAL ANALYSIS

All experiments were performed in biological replicates of at least three repeats ($n > 3$). Statistical analysis was performed using GraphPad Prism (version 8.4.3). Statistics are represented as mean ± standard error of the mean (SEM) as indicated. Statistical significance was calculated using Students t-test, analysis of variance (ANOVA) with Tukey's or Sidak's *post hoc* test for multiple comparisons, logrank test (for Kaplan-Meier survival curves), and χ^2 test for non-parametric comparisons. Statistical significance was set at $p<0.05$ (*, $p<0.05$; **, $p<0.01$; ***, $p<0.001$; ****, $p<0.0001$).

ADDITIONAL RESOURCES

Requests for additional resources should be addressed to the lead contact, Dimitris Placantonakis (dimitris.placantonakis@nyulangone.org).

Supplementary Material

Refer to Web version on PubMed Central for supplementary material.

ACKNOWLEDGMENTS

scRNA-seq data in GBM were obtained from the Single Cell Portal of the Broad Institute (https://singlecell.broadinstitute.org/single_cell/study/SCP393/single-cell-rna-seq-of-adult-and-pediatric-glioblastoma). GBM bulk RNA-seq, patient survival, and microarray data were obtained from the TCGA, CGGA, and Rembrandt databases, using the Xena browser (https://xenabrowser.net/) and Gliovis[43] for visualization and analysis. Sequencing aberration decomposition was performed with TIDE[33] (http://shinyapps.datacurators.nl/tide/). We thank the Microscopy and Flow Cytometry core facilities at the NYU Grossman School of Medicine. This study was supported by NIH/NINDS R01 NS102665, NIH/NINDS R01 NS124920, NIH/NINDS R21 NS126806, and (NYSTEM) IIRP C32595GG to D.G.P. D.G.P. was also supported by NIH/NIBIB R01 EB028774, NIH/NCI R21CA263402, NIH/NCATS 2UL1TR001445, NYU Grossman School of Medicine, NYU Perlmutter Cancer Center, and DFG (German Research Foundation) FOR2149. G.S. was supported by a DFG post-doctoral fellowship

(STE 2843/1–1). We acknowledge support from NIH 1S10RR027990 to T.A.N. Core facilities were supported in part by Cancer Center Support Grant P30CA016087 to the Perlmutter Cancer Center of NYU Grossman School of Medicine.

REFERENCES

1. Krishnan A, Nijmeijer S, de Graaf C, and Schiöth HB (2016). Classification, Nomenclature, and Structural Aspects of Adhesion GPCRs. Handb. Exp. Pharmacol 234, 15–41. 10.1007/978-3-319-41523-9_2. [PubMed: 27832482]
2. Hamann J, Aust G, Araç D, Engel FB, Formstone C, Fredriksson R, Hall RA, Harty BL, Kirchhoff C, Knapp B, et al. (2015). International Union of Basic and Clinical Pharmacology. XCIV. Adhesion G protein-coupled receptors. Pharmacol. Rev 67, 338–367. 10.1124/pr.114.009647. [PubMed: 25713288]
3. Scholz N, Langenhan T, and Schöneberg T (2019). Revisiting the classification of adhesion GPCRs. Ann. N. Y. Acad. Sci 1456, 80–95. 10.1111/nyas.14192. [PubMed: 31365134]
4. Kaczmarek I, Suchý T, Prömel S, Schöneberg T, Liebscher I, and Thor D (2021). The relevance of adhesion G protein-coupled receptors in metabolic functions. Biol. Chem 403, 195–209. 10.1515/hsz-2021-0146. [PubMed: 34218541]
5. Langenhan T (2020). Adhesion G protein-coupled receptors-Candidate metabotropic mechanosensors and novel drug targets. Basic Clin. Pharmacol. Toxicol 126 (Suppl 6), 5–16. 10.1111/bcpt.13223.
6. Einspahr JM, and Tilley DG (2022). Pathophysiological impact of the adhesion G protein-coupled receptor family. Am. J. Physiol. Cell Physiol 323, C640–c647. 10.1152/ajpcell.00445.2021. [PubMed: 35848619]
7. Araç D, Boucard AA, Bolliger MF, Nguyen J, Soltis SM, Sudhof TC, and Brunger AT (2012). A novel evolutionarily conserved domain of cell-adhesion GPCRs mediates autoproteolysis. EMBO J 31, 1364–1378. 10.1038/emboj.2012.26. [PubMed: 22333914]
8. Frenster JD, Stephan G, Ravn-Boess N, Bready D, Wilcox J, Kieslich B, Wilde C, Sträter N, Wiggin GR, Liebscher I, et al. (2021). Functional impact of intramolecular cleavage and dissociation of adhesion G protein-coupled receptor GPR133 (ADGRD1) on canonical signaling. J. Biol. Chem 296, 100798. 10.1016/j.jbc.2021.100798. [PubMed: 34022221]
9. Liebscher I, Schön J, Petersen SC, Fischer L, Auerbach N, Demberg LM, Mogha A, Cöster M, Simon KU, Rothemund S, et al. (2014). A tethered agonist within the ectodomain activates the adhesion G protein-coupled receptors GPR126 and GPR133. Cell Rep 9, 2018–2026. 10.1016/j.celrep.2014.11.036. [PubMed: 25533341]
10. Barros-Á lvarez X, Nwokonko RM, Vizurraga A, Matzov D, He F, Papasergi-Scott MM, Robertson MJ, Panova O, Yardeni EH, Seven AB, et al. (2022). The tethered peptide activation mechanism of adhesion GPCRs. Nature 604, 757–762. 10.1038/s41586-022-04575-7. [PubMed: 35418682]
11. Qu X, Qiu N, Wang M, Zhang B, Du J, Zhong Z, Xu W, Chu X, Ma L, Yi C, et al. (2022). Structural basis of tethered agonism of the adhesion GPCRs ADGRD1 and ADGRF1. Nature 604, 779–785. 10.1038/s41586-022-04580-w. [PubMed: 35418679]
12. Ping YQ, Xiao P, Yang F, Zhao RJ, Guo SC, Yan X, Wu X, Zhang C, Lu Y, Zhao F, et al. (2022). Structural basis for the tethered peptide activation of adhesion GPCRs. Nature 604, 763–770. 10.1038/s41586-022-04619-y. [PubMed: 35418678]
13. Xiao P, Guo S, Wen X, He QT, Lin H, Huang SM, Gou L, Zhang C, Yang Z, Zhong YN, et al. (2022). Tethered peptide activation mechanism of the adhesion GPCRs ADGRG2 and ADGRG4. Nature 604, 771–778. 10.1038/s41586-022-04590-8. [PubMed: 35418677]
14. Bayin NS, Frenster JD, Kane JR, Rubenstein J, Modrek AS, Baitalmal R, Dolgalev I, Rudzenski K, Scarabottolo L, Crespi D, et al. (2016). GPR133 (ADGRD1), an adhesion G-protein-coupled receptor, is necessary for glioblastoma growth. Oncogenesis 5, e263. 10.1038/oncsis.2016.63. [PubMed: 27775701]
15. Frenster JD, Inocencio JF, Xu Z, Dhaliwal J, Alghamdi A, Zagzag D, Bayin NS, and Placantonakis DG (2017). GPR133 Promotes Glioblastoma Growth in Hypoxia. Neurosurgery 64, 177–181. 10.1093/neuros/nyx227. [PubMed: 28899043]

16. Frenster JD, Kader M, Kamen S, Sun J, Chiriboga L, Serrano J, Bready D, Golub D, Ravn-Boess N, Stephan G, et al. (2020). Expression profiling of the adhesion G protein-coupled receptor GPR133 (ADGRD1) in glioma subtypes. Neurooncol. Adv 2, vdaa053. 10.1093/noajnl/vdaa053. [PubMed: 32642706]
17. Stephan G, Frenster JD, Liebscher I, and Placantonakis DG (2022). Activation of the adhesion G protein-coupled receptor GPR133 by antibodies targeting its N-terminus. J. Biol. Chem 298, 101949. 10.1016/j.jbc.2022.101949. [PubMed: 35447113]
18. Frenster JD, Erdjument-Bromage H, Stephan G, Ravn-Boess N, Wang S, Liu W, Bready D, Wilcox J, Kieslich B, Jankovic M, et al. (2023). PTK7 is a positive allosteric modulator of GPR133 signaling in glioblastoma. Cell Rep 42, 112679. 10.1016/j.celrep.2023.112679. [PubMed: 37354459]
19. Bohnekamp J, and Schöneberg T (2011). Cell adhesion receptor GPR133 couples to Gs protein. J. Biol. Chem 286, 41912–41916. 10.1074/jbc.C111.265934. [PubMed: 22025619]
20. Bianchi E, Sun Y, Almansa-Ordonez A, Woods M, Goulding D, Martinez-Martin N, and Wright GJ (2021). Control of oviductal fluid flow by the G-protein coupled receptor Adgrd1 is essential for murine embryo transit. Nat. Commun 12, 1251. 10.1038/s41467-021-21512-w. [PubMed: 33623007]
21. Giordano F, Saheki Y, Idevall-Hagren O, Colombo SF, Pirruccello M, Milosevic I, Gracheva EO, Bagriantsev SN, Borgese N, and De Camilli P (2013). PI(4,5)P(2)-dependent and Ca(2+)-regulated ER-PM interactions mediated by the extended synaptotagmins. Cell 153, 1494–1509. 10.1016/j.cell.2013.05.026. [PubMed: 23791178]
22. Saheki Y, Bian X, Schauder CM, Sawaki Y, Surma MA, Klose C, Pincet F, Reinisch KM, and De Camilli P (2016). Control of plasma membrane lipid homeostasis by the extended synaptotagmins. Nat. Cell Biol 18, 504–515. 10.1038/ncb3339. [PubMed: 27065097]
23. Fernandez-Busnadiego R, Saheki Y, and De Camilli P (2015). Three-dimensional architecture of extended synaptotagmin-mediated endoplasmic reticulum-plasma membrane contact sites. Proc. Natl. Acad. Sci. USA 112, E2004–E2013. 10.1073/pnas.1503191112. [PubMed: 25787254]
24. Bian X, Saheki Y, and De Camilli P (2018). Ca(2+) releases E-Syt1 auto-inhibition to couple ER-plasma membrane tethering with lipid transport. EMBO J 37, 219–234. 10.15252/embj.201797359. [PubMed: 29222176]
25. Ge J, Bian X, Ma L, Cai Y, Li Y, Yang J, Karatekin E, De Camilli P, and Zhang Y (2022). Stepwise membrane binding of extended synaptotagmins revealed by optical tweezers. Nat. Chem. Biol 18, 313–320. 10.1038/s41589-021-00914-3. [PubMed: 34916620]
26. Chang CL, Hsieh TS, Yang TT, Rothberg KG, Azizoglu DB, Volk E, Liao JC, and Liou J (2013). Feedback regulation of receptor-induced Ca2+ signaling mediated by E-Syt1 and Nir2 at endoplasmic reticulum-plasma membrane junctions. Cell Rep 5, 813–825. 10.1016/j.celrep.2013.09.038. [PubMed: 24183667]
27. Min SW, Chang WP, and Südhof TC (2007). E-Syts, a family of membranous Ca2+-sensor proteins with multiple C2 domains. USAProc. Natl. Acad. Sci. USA 104, 3823–3828. 10.1073/pnas.0611725104.
28. Idevall-Hagren O, Lü A, Xie B, and De Camilli P (2015). Triggered Ca2+ influx is required for extended synaptotagmin 1-induced ER-plasma membrane tethering. EMBO J 34, 2291–2305. 10.15252/embj.201591565. [PubMed: 26202220]
29. Schauder CM, Wu X, Saheki Y, Narayanaswamy P, Torta F, Wenk MR, De Camilli P, and Reinisch KM (2014). Structure of a lipid-bound extended synaptotagmin indicates a role in lipid transfer. Nature 510, 552–555. 10.1038/nature13269. [PubMed: 24847877]
30. Kang F, Zhou M, Huang X, Fan J, Wei L, Boulanger J, Liu Z, Salamero J, Liu Y, and Chen L (2019). E-syt1 Re-arranges STIM1 Clusters to Stabilize Ring-shaped ER-PM Contact Sites and Accelerate Ca(2+) Store Replenishment. Sci. Rep 9, 3975. 10.1038/s41598-019-40331-0. [PubMed: 30850711]
31. Kim DI, Jensen SC, Noble KA, Kc B, Roux KH, Motamedchaboki K, and Roux KJ (2016). An improved smaller biotin ligase for BioID proximity labeling. Mol. Biol. Cell 27, 1188–1196. 10.1091/mbc.E15-12-0844. [PubMed: 26912792]

32. Soucy TA, Smith PG, Milhollen MA, Berger AJ, Gavin JM, Adhikari S, Brownell JE, Burke KE, Cardin DP, Critchley S, et al. (2009). An inhibitor of NEDD8-activating enzyme as a new approach to treat cancer. Nature 458, 732–736. 10.1038/nature07884. [PubMed: 19360080]
33. Brinkman EK, Chen T, Amendola M, and van Steensel B (2014). Easy quantitative assessment of genome editing by sequence trace decomposition. Nucleic Acids Res 42, e168. 10.1093/nar/gku936. [PubMed: 25300484]
34. Aktasx T, Avsar Ilik I, Maticzka D, Bhardwaj V, Pessoa Rodrigues C, Mittler G, Manke T, Backofen R, and Akhtar A (2017). DHX9 suppresses RNA processing defects originating from the Alu invasion of the human genome. Nature 544, 115–119. 10.1038/nature21715. [PubMed: 28355180]
35. Bekker-Jensen DB, Kelstrup CD, Batth TS, Larsen SC, Haldrup C, Bramsen JB, Sørensen KD, Høyer S, Ørntoft TF, Andersen CL, et al. (2017). An Optimized Shotgun Strategy for the Rapid Generation of Comprehensive Human Proteomes. Cell Syst 4, 587–599.e4. 10.1016/j.cels.2017.05.009. [PubMed: 28601559]
36. Liou J, Kim ML, Heo WD, Jones JT, Myers JW, Ferrell JE Jr., and Meyer T (2005). STIM is a Ca2+ sensor essential for Ca2+-store-depletion-triggered Ca2+ influx. Curr. Biol 15, 1235–1241. 10.1016/j.cub.2005.05.055. [PubMed: 16005298]
37. Lé rias JR, Pinto MC, Botelho HM, Awatade NT, Quaresma MC, Silva IAL, Wanitchakool P, Schreiber R, Pepperkok R, Kunzelmann K, and Amaral MD (2018). A novel microscopy-based assay identifies extended synaptotagmin-1 (ESYT1) as a positive regulator of anoctamin 1 traffic. Biochim. Biophys. Acta Mol. Cell Res 1865, 421–431. 10.1016/j.bbamcr.2017.11.009. [PubMed: 29154949]
38. Venkataramani V, Tanev DI, Strahle C, Studier-Fischer A, Fankhauser L, Kessler T, Körber C, Kardorff M, Ratliff M, Xie R, et al. (2019). Glutamatergic synaptic input to glioma cells drives brain tumour progression. Nature 573, 532–538. 10.1038/s41586-019-1564-x. [PubMed: 31534219]
39. Venkataramani V, Yang Y, Schubert MC, Reyhan E, Tetzlaff SK, Wißmann N, Botz M, Soyka SJ, Beretta CA, Pramatarov RL, et al. (2022). Glioblastoma hijacks neuronal mechanisms for brain invasion. Cell 185, 2899–2917.e31. 10.1016/j.cell.2022.06.054. [PubMed: 35914528]
40. Venkatesh HS, Morishita W, Geraghty AC, Silverbush D, Gillespie SM, Arzt M, Tam LT, Espenel C, Ponnuswami A, Ni L, et al. (2019). Electrical and synaptic integration of glioma into neural circuits. Nature 573, 539–545. 10.1038/s41586-019-1563-y. [PubMed: 31534222]
41. Hausmann D, Hoffmann DC, Venkataramani V, Jung E, Horschitz S, Tetzlaff SK, Jabali A, Hai L, Kessler T, Azórin, D.D., et al. (2023). Autonomous rhythmic activity in glioma networks drives brain tumour growth. Nature 613, 179–186. 10.1038/s41586-022-05520-4. [PubMed: 36517594]
42. Xie B, Nguyen PM, and Idevall-Hagren O (2019). Feedback regulation of insulin secretion by extended synaptotagmin-1. Faseb. J 33, 4716–4728. 10.1096/fj.201801878R. [PubMed: 30589572]
43. Bowman RL, Wang Q, Carro A, Verhaak RGW, and Squatrito M (2017). GlioVis data portal for visualization and analysis of brain tumor expression datasets. Neuro Oncol 19, 139–141. 10.1093/neuonc/now247. [PubMed: 28031383]
44. Frenster JD, and Placantonakis DG (2018). Establishing Primary Human Glioblastoma Tumorsphere Cultures from Operative Specimens. Methods Mol. Biol 1741, 63–69. 10.1007/978-1-4939-7659-1_4. [PubMed: 29392690]
45. Xu Z, Kader M, Sen R, and Placantonakis DG (2018). Orthotopic Patient-Derived Glioblastoma Xenografts in Mice. Methods Mol. Biol 1741, 183–190. 10.1007/978-1-4939-7659-1_14. [PubMed: 29392700]
46. Frenster JD, Inocencio J, and Placantonakis DG (2018). Lentiviral Transduction of Primary Human Glioblastoma Cultures. Methods Mol. Biol 1741, 81–89. 10.1007/978-1-4939-7659-1_6. [PubMed: 29392692]
47. Xu Y, Erdjument-Bromage H, Phoon CKL, Neubert TA, Ren M, and Schlame M (2021). Cardiolipin remodeling enables protein crowding in the inner mitochondrial membrane. EMBO J 40, e108428. 10.15252/embj.2021108428. [PubMed: 34661298]

48. Rappsilber J, Mann M, and Ishihama Y (2007). Protocol for micro-purification, enrichment, pre-fractionation and storage of peptides for proteomics using StageTips. Nat. Protoc 2, 1896–1906. 10.1038/nprot.2007.261. [PubMed: 17703201]

49. Cox J, Neuhauser N, Michalski A, Scheltema RA, Olsen JV, and Mann M (2011). Andromeda: a peptide search engine integrated into the MaxQuant environment. J. Proteome Res 10, 1794–1805. 10.1021/pr101065j. [PubMed: 21254760]

50. Tyanova S, Temu T, and Cox J (2016). The MaxQuant computational platform for mass spectrometry-based shotgun proteomics. Nat. Protoc 11, 2301–2319. 10.1038/nprot.2016.136. [PubMed: 27809316]

51. Cox J, Hein MY, Luber CA, Paron I, Nagaraj N, and Mann M (2014). Accurate proteome-wide label-free quantification by delayed normalization and maximal peptide ratio extraction, termed MaxLFQ. Mol. Cell. Proteomics 13, 2513–2526. 10.1074/mcp.M113.031591. [PubMed: 24942700]

52. Berlin S, Carroll EC, Newman ZL, Okada HO, Quinn CM, Kallman B, Rockwell NC, Martin SS, Lagarias JC, and Isacoff EY (2015). Photoactivatable genetically encoded calcium indicators for targeted neuronal imaging. Nat. Methods 12, 852–858. 10.1038/nmeth.3480. [PubMed: 26167640]

53. Liberti WA 3rd, Markowitz JE, Perkins LN, Liberti DC, Leman DP, Guitchounts G, Velho T, Kotton DN, Lois C, and Gardner TJ (2016). Unstable neurons underlie a stable learned behavior. Nat. Neurosci 19, 1665–1671. 10.1038/nn.4405. [PubMed: 27723744]

54. Frenster JD, and Placantonakis DG (2018). Bioluminescent In Vivo Imaging of Orthotopic Glioblastoma Xenografts in Mice. Methods Mol. Biol 1741, 191–198. 10.1007/978-1-4939-7659-1_15. [PubMed: 29392701]

Highlights

- Extended synaptotagmin 1 (ESYT1) and adhesion GPCR GPR133 interact in glioblastoma
- The GPR133-ESYT1 interaction requires the Ca^{2+}-sensing C2C domain of ESYT1
- ESYT1 suppresses GPR133 signaling
- Increases in cytosolic Ca^{2+} relieve signaling-suppressive effects of ESYT1

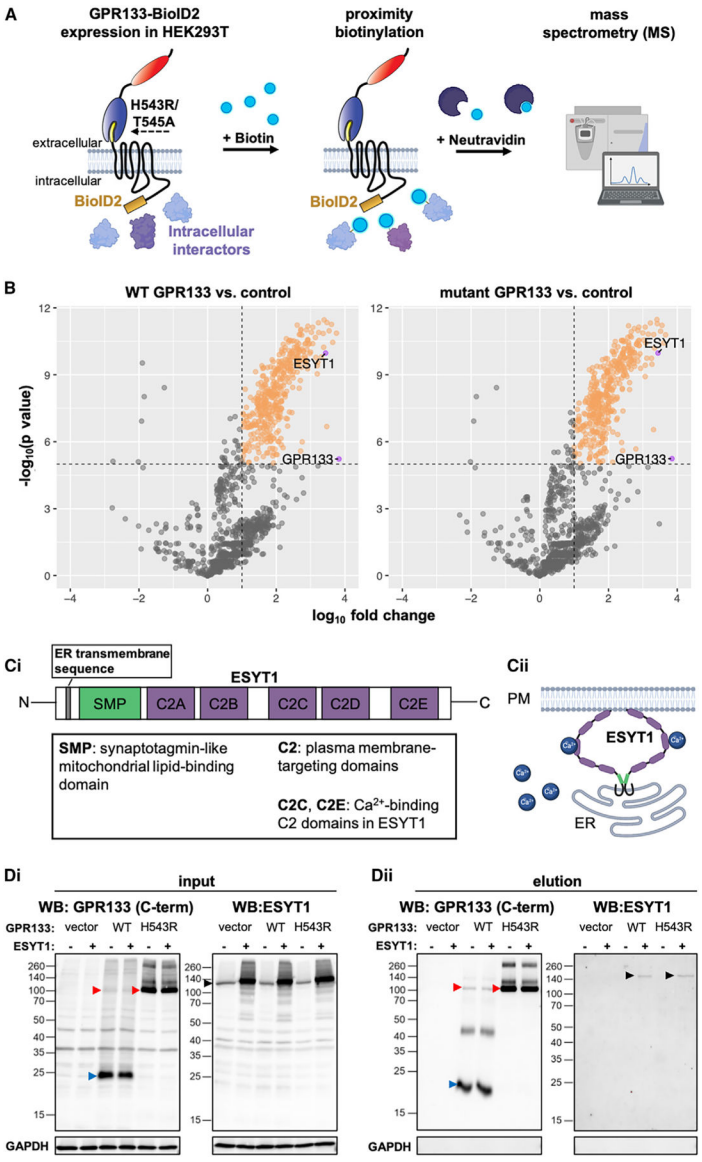

Figure 1. Identification of ESYT1 as a cytosolic interaction partner of GPR133

(A) Experimental design: BioID2-fusion constructs of wild-type (WT) or mutant (H543R/T545A) GPR133 were overexpressed in HEK293T cells. Following treatment with biotin, biotinylated proteins were purified using NeutrAvidin beads. Purified proteins were analyzed by mass spectrometry.

(B) Volcano plots showing enriched (orange) proteins in the comparisons of WT or mutant GPR133 to control. The dashed lines show a *p*-value cutoff of $<10^{-5}$ and $\log_{10}$ fold-change cutoff of >1. GPR133 and ESYT1 are identified on the plots.

(C) Structure and function of ESYT1. (i) Structural domains of ESYT1. (ii) ESYT1 dimers form ER-PM tethers in response to elevations in cytosolic Ca^{2+}.

(D) Co-purification confirms binding of ESYT1 to Twin-Strep-tagged GPR133, both WT and the uncleavable H543R mutant. (i) Input samples: whole-cell lysates of HEK293T cells expressing WT GPR133 or the cleavage-deficient mutant GPR133 (H543R) with a

C-terminal Twin-Strep-tag following transfection with ESYT1 (red arrowheads, full-length uncleaved GPR133; blue arrowheads, GPR133 CTF after cleavage; black arrowheads, ESYT1). (ii) Elution samples following Strep-Tactin purification. The ESYT1 bands in elution samples (ii) ran at a slightly higher apparent molecular weight than the ESYT1 bands in input samples (i), possibly because of the impact of reagents used for the co-purification and elution on electrophoretic mobility. WB, western blot; C-term, antibody against the cytosolic C terminus of GPR133.

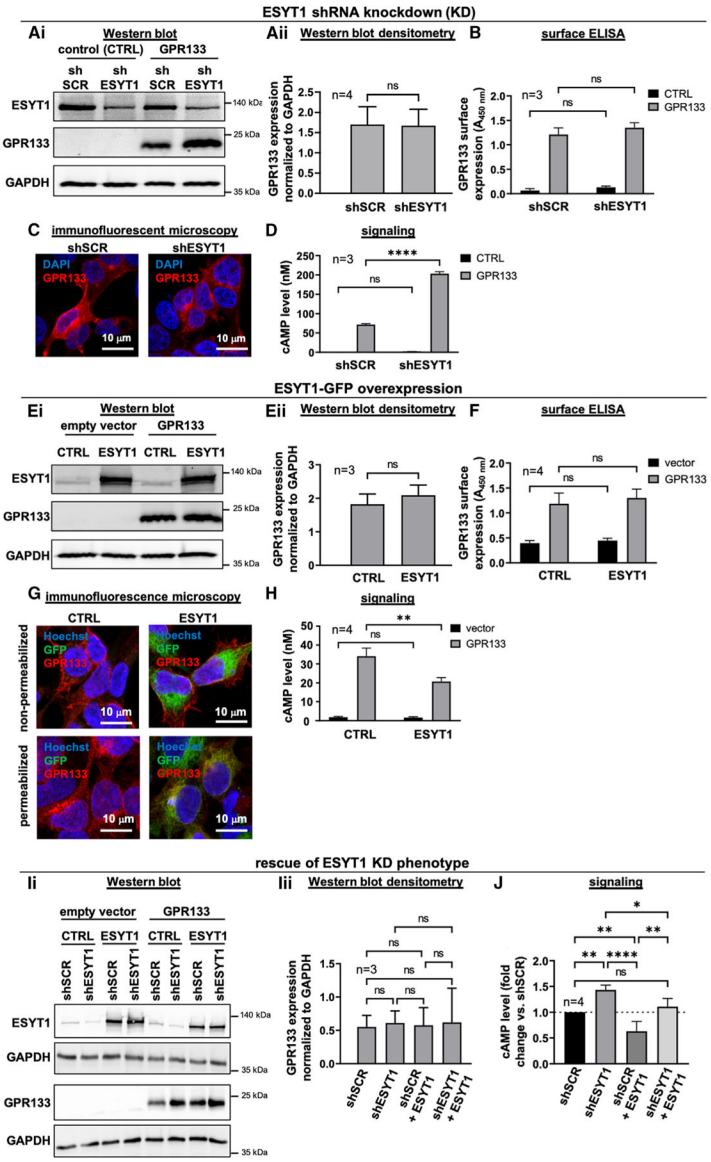

Figure 2. Effects of ESYT1 knockdown and overexpression on GPR133 signaling

(A–D) ESYT1 knockdown. (A) Western blot confirms reduced levels of endogenous ESYT1, following its knockdown (shESYT1) compared to the control (shSCR), and stable expression of GPR133, in transduced HEK293T cells. (i) Representative western blot membrane. (ii) Densitometry of the GPR133 signal confirms unchanged GPR133 expression following the knockdown of ESYT1 (shESYT1) compared to the control (shSCR) (paired t test, $p = 0.8986$). Bars represent mean ± standard error of the mean (SEM) of four experiments. ns, not significant. (B) GPR133 surface expression is not affected by ESYT1 knockdown in ELISA (two-way ANOVA, $p > 0.05$). ns, not significant; $A_{450\ nm}$, absorbance/optical density at 450 nm. Bars represent mean ± SEM of three experiments. (C) Immunofluorescent staining shows no change in the subcellular localization of GPR133 following knockdown of ESYT1 compared to the control. (D) Intracellular cAMP levels increase significantly in GPR133-expressing HEK293T cells after knockdown of ESYT1

compared to the control (two-way ANOVA $F_{(1,8)} = 503.2$, $p < 0.0001$; Sidak's *post hoc* test, GPR133 + shSCR vs. GPR133 + shESYT1, $p < 0.0001$). Bars represent mean ± SEM of three experiments.

(E–H) ESYT1-GFP overexpression. (i) Western blot confirms increased ESYT1-GFP protein levels following transfection of GPR133-expressing cells. (ii) GPR133 expression levels are not affected in HEK293T cells overexpressing ESYT1 in quantitative densitometry comparisons (paired t test, $p = 0.3203$). Bars represent mean ± SEM of three experiments. ns, not significant. (F) GPR133 surface expression remains unchanged following overexpression of ESYT1-GFP (two-way ANOVA, $p > 0.05$). Bars represent mean ± SEM of four experiments. ns, not significant; $A_{450\ nm}$, absorbance/optical density at 450 nm. (G) Immunofluorescent staining of both permeabilized and non-permeabilized HEK293T cells expressing GPR133 combined with either empty vector or ESYT1-GFP. The subcellular distribution of GPR133 immunoreactivity is unchanged by the presence of ESYT1-GFP. The permeabilized cells also show co-localization in ESYT1-GFP and GPR133 immunoreactivity within intracellular compartments. (H) Intracellular cAMP levels significantly decrease in GPR133-expressing HEK293T cells following overexpression of ESYT1-GFP compared to the control (two-way ANOVA $F_{(1,12)} = 7.928$, $p < 0.0156$; Sidak's *post hoc* test, GPR133 + CTRL vs. GPR133 + ESYT1, $p = 0.0041$). Bars represent mean ± SEM of four experiments. ns, not significant.

(I and J) ESYT1 overexpression rescues the effect of ESYT1 knockdown in GPR133-overexpressing cells. (i) Western blot confirming ESYT1 knockdown and overexpression in HEK293T cells and HEK293T cells overexpressing GPR133. (ii) Expression levels of GPR133 were not affected following knockdown or overexpression of ESYT1 in quantitative densitometry (one-way ANOVA, $p > 0.05$). Bars represent mean ± SEM of three experiments. ns, not significant. (J) Intracellular cAMP levels of GPR133-expressing HEK293T cells are normalized to shSCR. Bars represent mean ± SEM of four experiments. Compared to the control (shSCR), GPR133 signaling increases significantly following transduction with shESYT1 and decreases significantly following transfection with ESYT1. ESYT1 overexpression rescues the increase in cAMP levels after ESYT1 KD (one-way ANOVA $F_{(3,12)} = 24.64$, $p < 0.0001$; Tukey's *post hoc* test, shSCR vs. shESYT1, $p = 0.0030$; shSCR vs. shSCR + ESYT1, $p = 0.0094$; shESYT1 vs. shSCR + ESYT1, $p < 0.0001$; shESYT1 vs. shESYT1 + ESYT1, $p = 0.0217$; shSCR + ESYT1 vs. shESYT1 + ESYT1, $p = 0.0014$). Bars represent mean ± SEM of four experiments. ns, not significant.

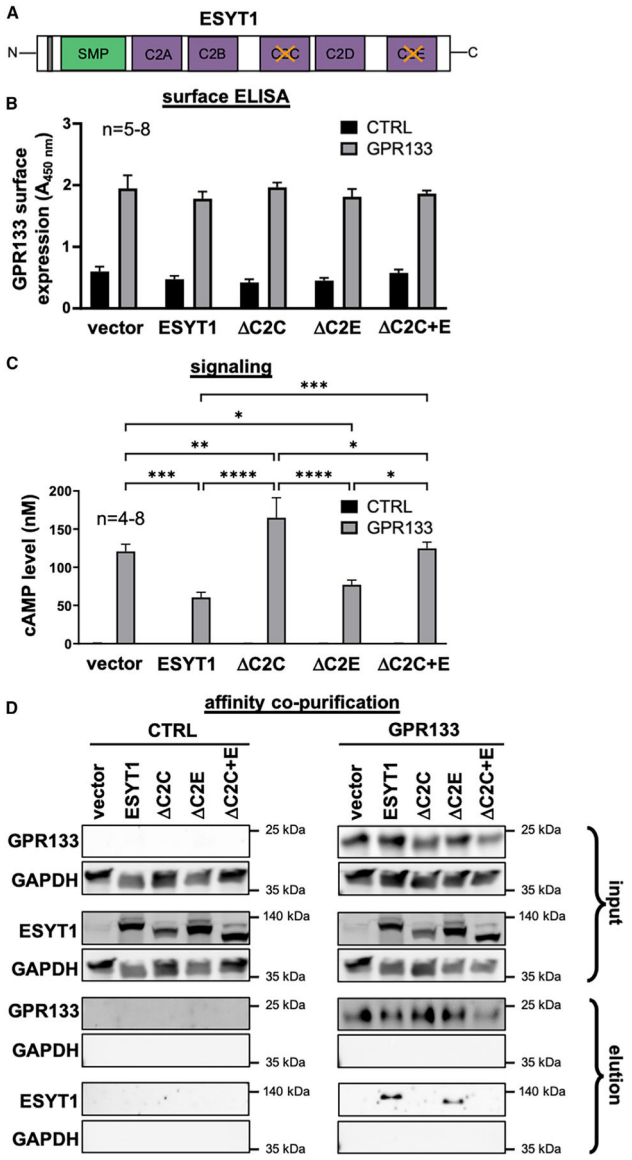

Figure 3. ESYT1 domains necessary for the interaction with GPR133

(A) Schematic showing ESYT1 deletion mutants used in this experiment.

(B) GPR133 surface expression in ELISAs following transfection of control HEK293T cells and HEK293T cells stably expressing GPR133 with different ESYT1 constructs. Overexpression of ESYT1, ΔC2C, ΔC2E, or ΔC2C+E did not affect GPR133 surface expression compared to the vector control (two-way ANOVA, $p > 0.05$). Bars represent the mean ± SEM of five to eight experiments. $A_{450\ nm}$, absorbance/optical density at 450 nm.

(C) Intracellular cAMP levels following transfection of HEK293T cells stably expressing GPR133 with WT or mutant ESYT1 constructs. Concentrations of cAMP were significantly decreased in GPR133-expressing cells after transfection with ESYT1 and ΔC2E compared to the vector control. Overexpression of ΔC2C increased cAMP levels compared to the vector control and WT ESYT1 in GPR133-expressing HEK293T cells (two-way ANOVA

$F_{(4,46)} = 9.471$, $p < 0.0001$; Sidak's *post hoc* test, GPR133 + vector vs. GPR133 + ESYT1, $p = 0.0001$; GPR133 + vector vs. GPR133 + ΔC2C, $p = 0.0080$; GPR133 + ESYT1 vs. GPR133 + ΔC2C, $p < 0.0001$; GPR133 + ESYT1 vs. GPR133 + ΔC2C+E, $p = 0.0002$; GPR133 + ΔC2E vs. GPR133 + ΔC2C+E, $p = 0.0218$). Bars represent the mean ± SEM of five to eight experiments.

(D) Affinity purification analysis testing binding of different ESYT1 constructs to GPR133. Input samples represent whole-cell lysates of naive HEK293T cells and HEK293T cells stably overexpressing GPR133 transfected with WT or deletion ESYT1 constructs. Elution samples following Strep-Tactin purification demonstrate that ESYT1-specific bands are detected only in GPR133-expressing cells transfected with WT ESYT1 and ΔC2E, but not after transfection with ΔC2C or ΔC2C+E.

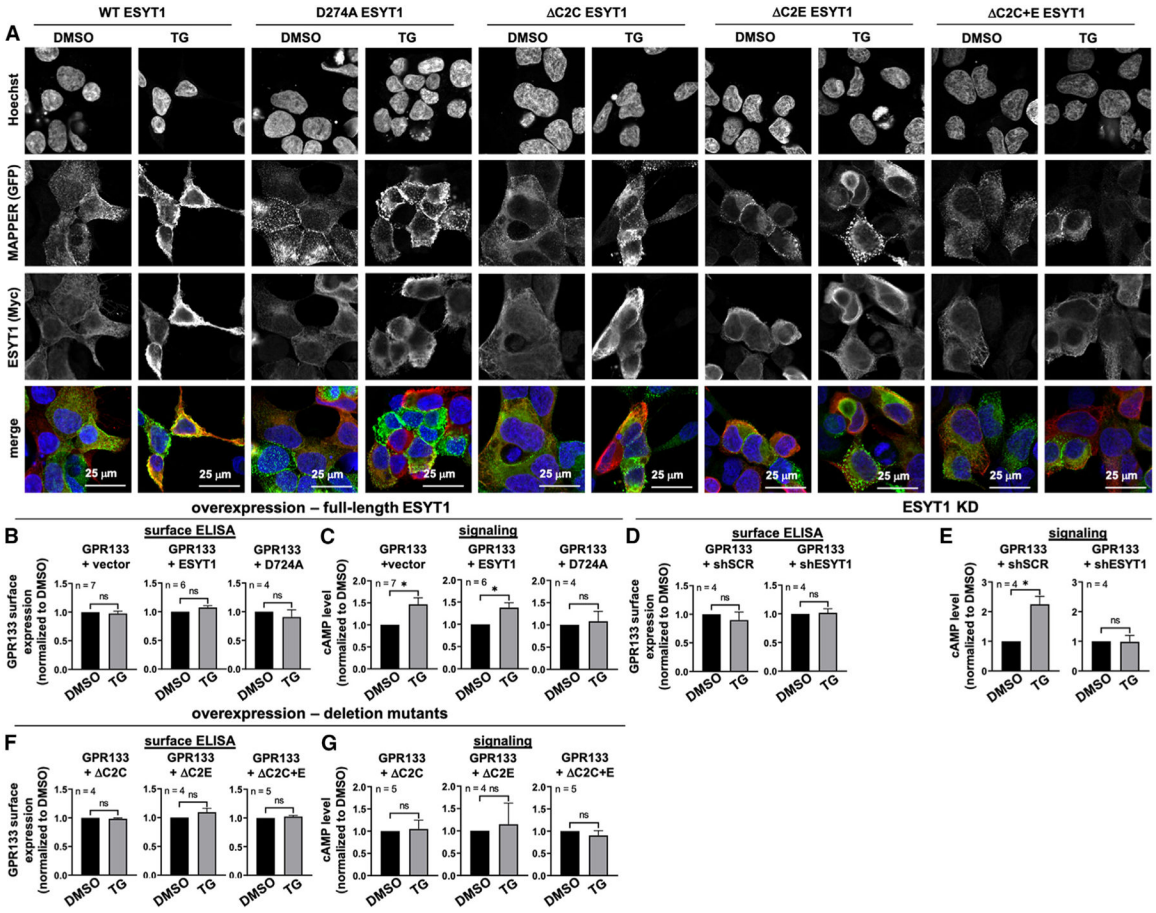

Figure 4. Intracellular Ca^{2+} increases impact GPR133 signaling dependent on ESYT1 expression

(A) Confocal images of HEK293 cells stably overexpressing MAPPER-GFP (green) transfected with Myc-tagged ESYT1 WT and mutant constructs (red) following treatment with DMSO or 1 μM TG to increase intracellular Ca^{2+} concentration. Yellow regions within the images represent overlap of MAPPER (green) and Myc-tagged ESYT1 (red), suggesting localization of ESYT1 at ER-PM junctions. The overlap is significantly more extensive following TG treatment of HEK293-MAPPER cells overexpressing WT ESYT1 rather than the mutant constructs.

(B–G) Effects of intracellular Ca^{2+} increases on GPR133 surface expression (B, D, and F) and cAMP levels (C, E, and G). (B and C) TG treatment of HEK293T cells stably expressing GPR133 transfected with vector or full-length WT or D724A mutant ESYT1. Bars represent mean ± SEM of four to seven experiments. (B) TG treatment had no effect on GPR133 surface expression in GPR133-expressing HEK293T cells transfected with vector, WT ESYT1, or D724A ESYT1 compared to treatment with DMSO (paired t test, $p > 0.05$). (C) TG treatment significantly increased cAMP levels in GPR133-expressing HEK293T cells transfected with vector and WT ESYT1 compared to treatment with DMSO (paired t test; GPR133 + vector, DMSO vs. TG, $p = 0.0210$; GPR133 + ESYT1, DMSO vs. TG, $p = 0.0189$). TG treatment did not affect GPR133 signaling following transfection of D724A ESYT1 (paired t test, $p > 0.05$). ns, not significant. (D and E) TG treatment of HEK293T cells transduced with shSCR or shESYT1 to knock down ESYT1. Bars represent mean

± SEM of four experiments. (D) TG treatment did not affect GPR133 surface expression compared to treatment with DMSO in GPR133-expressing HEK293T cells transduced with shSCR or shESYT (paired t test, $p > 0.05$). (E) TG treatment significantly increased cAMP concentrations compared to treatment with DMSO in HEK293T cells overexpressing GPR133 and transduced with shSCR (paired t test, $p = 0.018$). TG treatment had no effect on cAMP levels compared to DMSO following overexpression of GPR133 and ESYT1 KD (paired t test, $p > 0.05$). ns, not significant. (F and G) TG treatment of HEK293T cells stably expressing GPR133 transfected with ESYT1 deletion mutants ΔC2C, ΔC2E, or ΔC2C+E. Bars represent mean ± SEM of four or five experiments. (F) Treatment with TG had no effect on GPR133 surface expression in GPR133-expressing HEK293T cells transfected with ΔC2C, ΔC2E, or ΔC2C+E compared to treatment with DMSO (paired t test, $p > 0.05$). (G) TG treatment did not affect cAMP concentrations compared to treatment with DMSO in GPR133-expressing HEK293T cells transfected with ΔC2C, ΔC2E, or ΔC2C+E (paired t test, $p > 0.05$). ns, not significant.

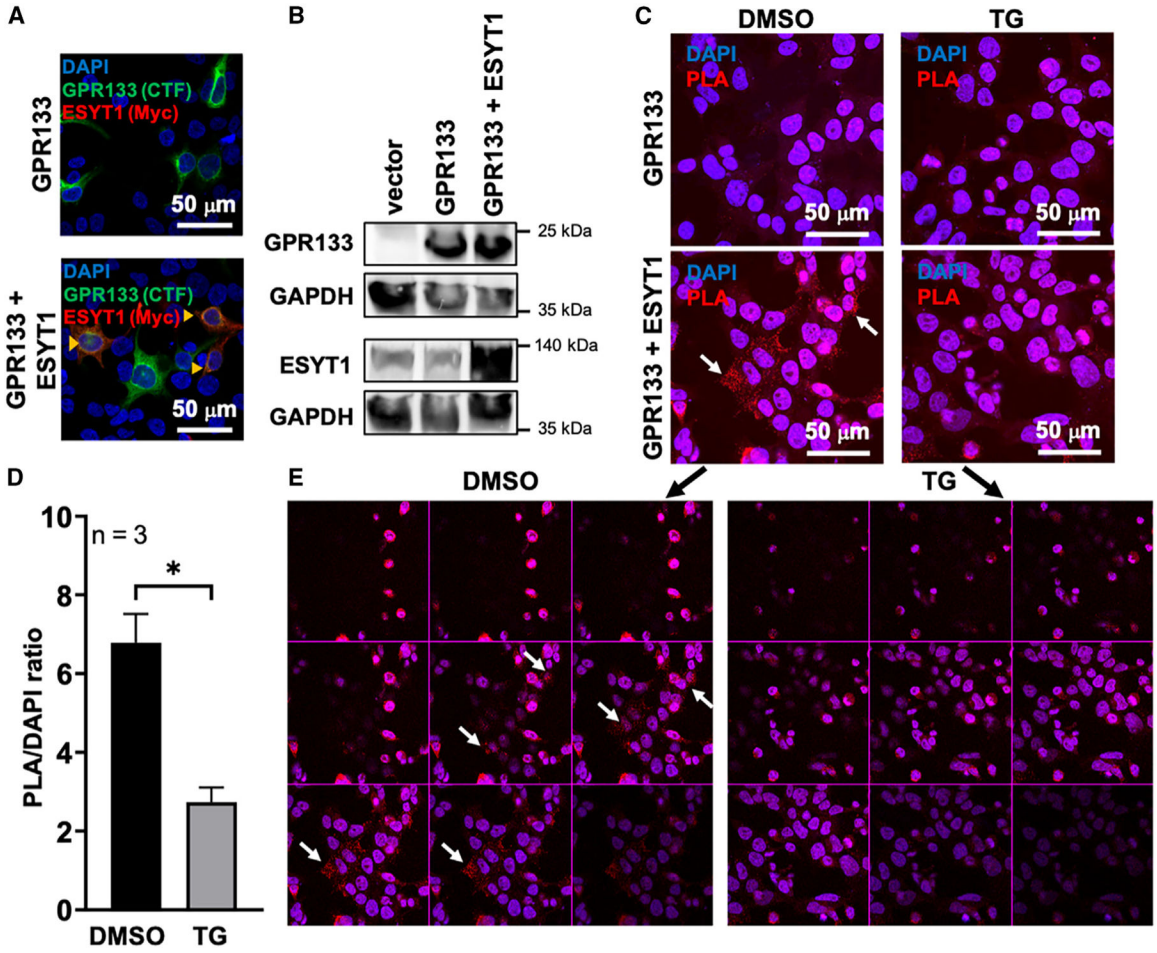

Figure 5. Intracellular Ca^{2+} increases disrupt binding of GPR133 and ESYT1

(A) Confocal images of HEK293T cells transfected with GPR133 alone (green) or co-transfected with GPR133 and Myc-tagged ESYT1 (red). In the co-transfection condition, the majority of transfected cells express both GPR133 and ESYT1 (orange arrowheads).

(B) Western blot confirms overexpression of GPR133 and ESYT1 in transfected HEK293T cells.

(C) Representative PLA images of HEK293T cells transfected with GPR133 or co-transfected with GPR133 and ESYT1. The red PLA signal (arrow) is only present in cells co-transfected with GPR133 and ESYT1. The signal is weaker in cells treated with 1 μM TG compared to cells treated with DMSO.

(D) Quantification of PLA-positive signals (red dots) over DAPI-positive cells overexpressing GPR133 and ESYT1. Bars represent the mean ± SEM of three experiments. The PLA/DAPI ratio is significantly decreased in TG-treated cells (paired t test, $p < 0.05$).

(E) Optical sections of GPR133 + ESYT1 images from the lower images in (C), detecting a strong PLA signal in DMSO-treated cells (arrows), but a weaker signal in TG-treated cells.

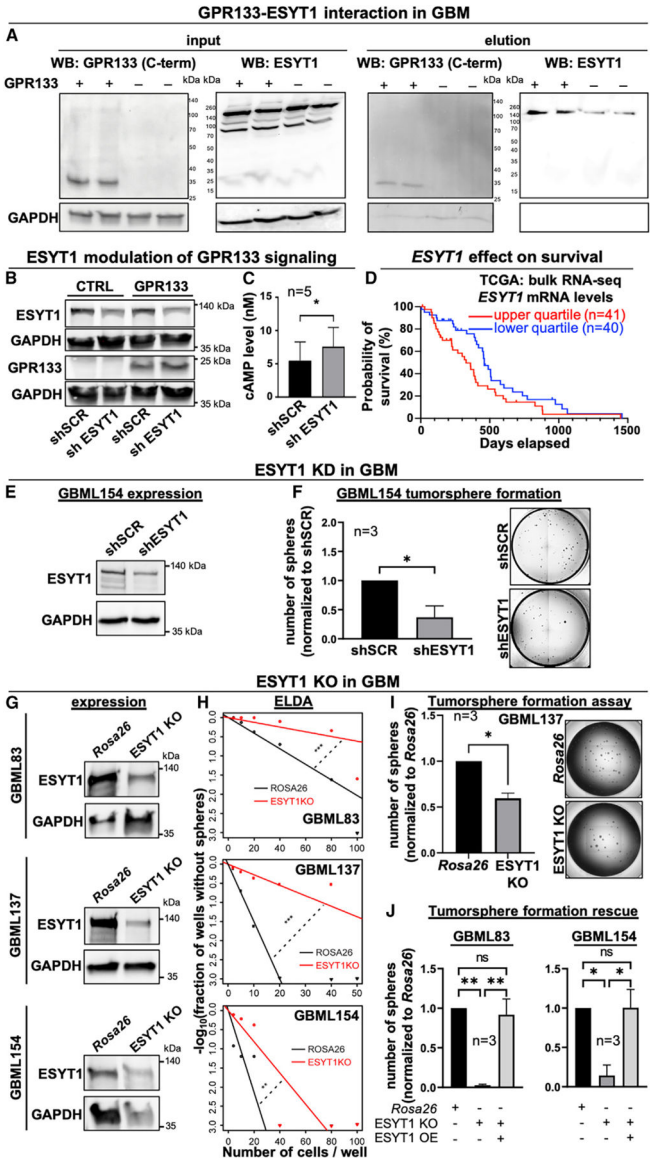

Figure 6. ESYT1 impacts GPR133 signaling and tumorsphere formation in patient-derived GBM cells

(A) Co-purification assay in GBML128 demonstrates interaction of endogenous ESYT1 with C-terminal Twin-Strep-tagged WT GPR133. Input samples (left) show whole-cell lysates of GBML128 GSCs expressing WT GPR133 with a C-terminal Twin-Strep-tag. Elution samples following Strep-Tactin purification are shown on the right. Note that endogenous ESYT1 shows some non-specific purification in the absence of Twin-Strep-tagged GPR133, but it is significantly enriched in the presence of GPR133. Two independent biological replicates were run on the same gel. WB, western blot; GPR133 C-term, antibody against the cytosolic C terminus of GPR133.

(B and C) GBML109 was transduced with lentivirus for overexpression of GPR133 and shRNA-mediated knockdown (KD) of ESYT1. (B) Western blot analysis using specific antibodies against ESYT1 (top) and GPR133 (bottom) confirms expression of ESYT1 in GBML109 transduced with the shSCR control and KD of ESYT1 following transduction

with shESYT1 in cells overexpressing GPR133 or an empty vector control. (C) Intracellular cAMP levels in GPR133-expressing GBML109 cells are significantly increased following KD of ESYT1 compared with the control (paired t test, $p < 0.05$). Bars represent the mean ± SEM of five experiments.

(D) Kaplan-Meier survival curves from the TCGA GBM dataset as a function of *ESYT1* mRNA levels in bulk RNA-seq of surgical specimens. Patients in the upper quartile of *ESYT1* mRNA levels experience shorter survival (median 329 days) relative to patients in the lower quartile (median 460 days) (log-rank Mantel-Cox test, $p = 0.0413$).

(E and F) Effects of ESYT1 KD by lentiviral transduction of shRNA in GBML154. (E) Western blot analysis confirms KD of ESYT1. (F) Tumorsphere formation is significantly reduced in GBML154 following KD of ESYT1 compared to the control shSCR (paired t test, $p = 0.0306$). Bars represent the mean ± SEM of three experiments. Representative examples are shown.

(G–J) Tumorsphere formation following the CRISPR-Cas9-mediated KO of ESYT1 in GBML83, GBML137, and GBML154. (G) Reduced ESYT1 expression, detected by western blot, following transduction with an ESYT1-specific CRISPR-Cas9 construct compared to the *Rosa26* control in three different GSC cultures. (H) Extreme limiting dilution assays (ELDAs) demonstrate impaired clonogenic tumorsphere formation after ESYT1 KO relative to the *Rosa26* control in three different GSC cultures. χ^2 test; $^{**}p < 0.01$, $^{***}p < 0.001$.

(I) Representative example of impaired tumorsphere formation following KO of ESYT1 in GBML137 GSCs (paired t test; $^{*}p < 0.05$). In this example, 500 cells were seeded per well. Bars represent the mean ± SEM of three experiments. (J) Overexpression (OE) of ESYT1 in GBML83 and GBML154 GSCs rescues the impairment in tumorsphere formation imparted by ESYT1 KO (GBML83: one-way ANOVA $F_{(2,6)} = 22.32$, $p = 0.0017$; Tukey's *post hoc* test, *Rosa26* vs. ESYT1 KO, $p = 0.0023$; ESYT1 KO vs. ESYT1 KO + ESYT1 OE, $p = 0.0036$; GBML154: one-way ANOVA $F_{(2,6)} = 10.30$, $p = 0.0115$; Tukey's *post hoc* test, *Rosa26* vs. ESYT1 KO, $p = 0.0183$; ESYT1 KO vs. ESYT1 KO + ESYT1 OE, $p = 0.0179$). Bars represent the mean ± SEM of three experiments. ns, not significant.

KEY RESOURCES TABLE

REAGENT or RESOURCE	SOURCE	IDENTIFIER
Antibodies		
Mouse monoclonal anti-GPR133 (NTF)	Not commercially available (Bayin et al.[14]) (Frenster et al.)[16]	Clone “8E3E8”
Rabbit polyclonal anti-GPR133 (C-terminus)	Sigma	HPA042395; RRID:AB_10796906
Rabbit polyclonal anti-ESYT1	Sigma	HPA016858; RRID:AB_1848404
Goat polyclonal anti-GAPDH	Invitrogen	PA1–9046; RRID:AB_1074703
Chicken polyclonal anti-GFP	Abcam	ab13970; RRID:AB_300798
Mouse monoclonal anti-Myc-tag (9B11)	Cell Signaling	2276S; RRID:AB_331783
Mouse monoclonal anti-FLAG-tag	Sigma	F3165-.2MG; RRID:AB_259529
Secondary donkey anti-mouse Alexa Fluor plus 488	Invitrogen	A32766; RRID:AB_2762823
Secondary goat anti-chicken Alexa Fluor plus 488	Invitrogen	A-11039; RRID:AB_2534096
Secondary donkey anti-rabbit Alexa Fluor plus 555	Invitrogen	A32794; RRID:AB_2762834
Secondary donkey anti-goat Alexa Fluor plus 647	Invitrogen	A32849; RRID:AB_2762840
Secondary chicken anti-mouse HRP-conjugated	Invitrogen	A15975; RRID:AB_2534649
Secondary chicken anti-rabbit HRP-conjugated	Invitrogen	A15987; RRID:AB_2534661
Chemicals, peptides, and recombinant proteins		
3-Isobutyl-1-methylxanthine (IBMX)	Sigma-Aldrich	I7018–100MG
DDM (n-dodecyl β-D-maltoside) (10%)	Thermo Fisher	BN2005
Dulbecco’s modified Eagle’s medium (DMEM)	Gibco	11965–118
Sodium pyruvate	Gibco	11360070
Fetal bovine serum (FBS)	Peak Serum	PS-FB2
Neurobasal Medium	Gibco	21103049
EGF	R&D	236-EG-01M
bFGF	R&D	233-FB-01M
GlutaMAX Supplement	Gibco	35050061
MEM Non-Essential Amino Acids	Gibco	11140050
N2 Supplement	Gibco	17-502-049
B27 Supplement	Gibco	12587010
Poly-L-Ornithine solution	Sigma	P4957–50ml
Laminin	Thermo Fisher	23017015

REAGENT or RESOURCE	SOURCE	IDENTIFIER
Lipofectamine 2000	Invitrogen	11668–019
Trypsin	Thermo Fisher	25300054
Accutase	Innovative Cell Technologies	AT104
Lenti-X Concentrator	Takara	631231
MagStrep “type3” XT magnetic beads	IBA	2-4090-002
10x Buffer W; Strep-Tactin Wash Buffer	IBA	2-1003-100
10x Buffer BXT	IBA	2-1042-025
BioLock Biotin blocking solution	IBA	2-0205-250
TMB Stabilized Chromogen	Thermo Fisher	SB02
ELISA Stop Solution	Thermo Fisher	SS04
Thapsigargin	Millipore Sigma	CAS 67526-95-8
G418	ThermoFisher	10131035
Puromycin dihydrochloride	Gibco	A1113803
D-Luciferin Potassium Salt	Gold Biotechnology	LUCK-300
Trizol	Invitrogen	15596026
DSS (disuccinimidyl suberate)	Thermo Fisher	21655
DNeasy Blood & Tissue Kit	Qiagen	69504
Direct-zol RNA Microprep kit	Zymo Research	R2062
iScript™ cDNA Synthesis Kit	Biorad	1708891
Critical commercial assays		
cAMP Gs Dynamic kit (HTRF)	CisBio	62AM4PEC
Duolink® *In Situ* PLA® Probe Anti-Mouse MINUS	Sigma	DUO92004
Duolink® *In Situ* PLA® Probe Anti-Rabbit PLUS	Sigma	DUO92002
Duolink® *In Situ* Detection Reagents Red	Sigma	DUO92008
Deposited data		
Proteomic data	MassIVE (UCSD, https://massive.ucsd.edu/ProteoSAFe/static/massive.jsp)	accession number MSV000091163
Experimental models: Cell lines		
Lenti-X 293T Cell Line	Takara	632180
Patient-derived GBM cultures	Not commercially available	GBML83/109/137/154
Experimental models: Mouse strains		
immunodeficient NSG (NOD.Cg-*Prkdc*^{scid}*Il2rg*^{tm1Wjl}/SzJ) mice	Jackson Labs	005557
Oligonucleotides		

REAGENT or RESOURCE	SOURCE	IDENTIFIER
CCGGCTCGTGTTGCCCAACCGATTACTCGAGTAATCGGTTGGGCAACACGAGTTTTTG	Eurofins Genomics	shESYT1_for
AATTCAAAAACTCGTGTTGCCCAACCGATTACTCGAGTAATCGGTTGGGCAACACGAG	Eurofins Genomics	shESYT1_rev
CCCTAGCCATTGCGCATCAT	Eurofins Genomics	guide1_ESYT1_KO_for
ATGATGCGCAATGGCTAGGG	Eurofins Genomics	guide1_ESYT1_KO_rev
GATCATGCATGAATTCGGATCCGGTGGAGGC	Eurofins Genomics	MCS-13X Linker-BioID2-HA_for
GATCATGCATTAAACCTATGCGTAATCCGG	Eurofins Genomics	MCS-13X Linker-BioID2-HA_rev
CTTTGACAAGGCCTTGGACAAGG	Eurofins Genomics	Mutation D724A_for
ACTTCAACCTCTAGCTCTTG	Eurofins Genomics	Mutation D724A_rev
GGTTAGCTCCTTCGGTCCTCC	Eurofins Genomics	Gibson Fragment1_for
GATAACACTGCGGCCAACTTACTTC	Eurofins Genomics	Gibson Fragment1_rev
AGAATCCCCAGAGAGGCAGCACCCTGGAGGATGTCCCATC	Eurofins Genomics	ΔC2C Gibson Fragment 2_for
GATGGGACATCCTCCAGGGTGCTGCCTCTCTGGGGATTCTC	Eurofins Genomics	ΔC2C Gibson Fragment 2_rev
CCAGCCGGGGACCTGATGGACAACAAGGACAAGGGCAGC	Eurofins Genomics	ΔC2E Gibson Fragment 2_for
GCTGCCCTTGTCCTTGTTGTCCATCAGGTCCCCGGCTGGAGCCTC	Eurofins Genomics	ΔC2E Gibson Fragment 2_rev
TATAGATCGACGCGACACCA	Eurofins Genomics	*OLIG2* qRT-PCR_for
CCTCGGACCCGAAAATCTGG	Eurofins Genomics	*OLIG2* qRT-PCR_rev
TACCCACCACAGCTGAAGAAG	Eurofins Genomics	*ESYT1* qRT-PCR_for
TTGGTACTGTAGACAGCCTTGC	Eurofins Genomics	*ESYT1* qRT-PCR_rev
ACAGAGCCTCGCCTTTGC	Eurofins Genomics	*ACTB* qRT-PCR_for
CCACCATCACGCCCTGG	Eurofins Genomics	*ACTB* qRT-PCR_rev
GAAACCAGAGGCGAGGGTGTGC	Eurofins Genomics	Forward primer for ESYT1 KO genotyping
TCTGGCCTACCTGCATGCCCTT	Eurofins Genomics	Reverse primer for ESYT1 KO genotyping
Recombinant DNA		
pLVX-EF1α-mCherry-N1 Vector	Takara	631986
MCS-13X Linker-BioID2-HA	(Kim et al)[31]	Addgene 80899
pLVX-GPR133-BioID2	This paper	N/A
pLVX-GPR133 (H543R/T545A)-BioID2	This paper	N/A
pLVX-GPR133-WT-Strep	(Frenster et al)[8]	N/A

REAGENT or RESOURCE	SOURCE	IDENTIFIER
Myc-ESYT1	(Giordano et al)[21]	Addgene 66833
Myc-OXSR1	Sino Biological	HG10727-NM
Myc-CYFIP2	Sino Biological	HG16749-NM
Myc-NAE1	Sino Biological	HG14282-NM
Myc-Miro2 (RHOT2)	(Fransson et al)[44]	Addgene 47891
EGFP-ESYT1	(Giordano et al)[21]	Addgene 66830
pLVX-Myc-ESYT1	This paper	N/A
pLVX-GPR133-WT	(Frenster et al)[8]	N/A
pLKO-shSCR	(Bayin et al)[14]	N/A
pLKO-shESYT1	This paper	N/A
LentiCRISPRv2GFP-Rosa26	This paper	N/A
LentiCRISPRv2GFP-ESYT1 KO (guide1_ESYT1)	This paper	N/A
pcDNA3-ADRB2	(Tang et al)[45]	Addgene 14697
pLVX-Myc-ESYT1 D724A	This paper	N/A
pLVX-Myc-ESYT1 ΔC2C	This paper	N/A
pLVX-Myc-ESYT1 ΔC2E	This paper	N/A
pLVX-Myc-ESYT1 ΔC2C+E	This paper	N/A
EGFP-C1-MAPPER	(Chang et al)[26]	Addgene 117721
pHAGE-RSV-TdTomato-2A-GCaMP6s	(Liberti et al)[46]	Addgene 80316